Geochemical element mobilisation by interaction of Bowland shale with acidic fluids

Yukun Ji [a], Jan A. I. Hennissen [b], Edward Hough [b], Veerle Vandeginste [a, c] *

[a] School of Chemistry, University of Nottingham, Nottingham, NG7 2RD, United Kingdom

[b] British Geological Survey, Environmental Science Centre, Keyworth, Nottingham, NG12 5GG, United Kingdom

[c] GeoEnergy Research Centre, Faculty of Engineering, University of Nottingham, Nottingham, NG7 2RD, United Kingdom

Abstract: Hydraulic fracturing is widely used to exploit unconventional hydrocarbon sources, to enhance exploitation of geothermal energy and to aid in carbon sequestration through underground storage of captured CO_2. The hydraulic fracturing fluids, which are commonly acidic, cause dissolution of minerals and desorption of elements which can lead to groundwater contamination. Batch reactor experiments were conducted to explore the interaction of simulated fracturing fluids with two end member compositions of basinal shales of the Bowland-Hodder unit (Carboniferous, UK) whereby the impact of temperature, fluid acidity, and rock/fluid ratio conditions were investigated. The results demonstrate that the fluid acidity is mainly controlled by the oxidative dissolution of pyrite and the dissolution of calcite, impacting mobilisation and fate of major and trace elements. The dissolution of calcite and pyrite significantly dominates the leaching of Sr and As, respectively. Generally, increased fluid acidity and temperature facilitate element mobilisation due to enhanced mineral dissolution and ion desorption, whereas higher rock/fluid ratio (higher mass of carbonate minerals) raises the buffering capacity and may promote the immobilisation of some metal ions by adsorption and precipitation (e.g. Ba, Pb, Fe, Al, and Mn). Moreover, the surface topography of different minerals in polished shale sample sections after fluid-rock interaction indicates that mineralogical compositions may play an important role in determining the pore structure. This research identifies chemical reaction pathways of geochemical elements (including contaminants) in fracturing fluids over a range of fluid chemistries and environmental conditions, and helps to evaluate element mobilisation from shale reservoirs with differing mineralogies.

Keywords: fracturing fluid; geochemical process; element mobilisation; water contamination; surface topography.

1 Introduction

Advances and development in horizontal drilling and hydraulic fracturing technologies have enabled the exploitation of the burning-clean shale gas from deep and low permeability shale reservoirs [1], whereas the environmental risks (potential groundwater contamination) caused by hydraulic fracturing has led to considerable concerns [2-4]. Organic-rich shale that has undergone sufficient burial acts as both the source and reservoir rock, and horizontal drilling alone is insufficient to achieve the economic exploitation of the gas resources because of the low permeability of shale reservoirs. Hence, high pressure (480 to 850 bar) hydraulic fracturing fluids are pumped and injected into the well to create fractures (migration paths) to increase the permeability of target shale reservoirs, and thus to stimulate the production of shale gas [5,6].

The typical constituents of hydraulic fracturing fluids for injection into the well include water, proppants, and

---

*Corresponding author.
E-mail address: veerle.vandeginste@gmail.com

31   chemicals [7]. The Council of Canadian Academies [8] indicates that the mass of chemicals in 20,000 m^3 of fracturing

32   fluid constitutes approximately 100 m^3 of acid, 1.5 million kg of proppant, 1,000 kg of friction reducer, 900 kg of

33   disinfectant, and 0.3 m^3 of corrosion inhibitor according to King [9]. Hydrochloric acid (HCl) is the major component

34   of fracturing fluids and can dissolve the reactive minerals and initiate cracks in the shale formation, thus providing a

35   dissolution space to maximise the growth and connectivity of the fracture networks [6,10-11]. Hence, the pressurised

36   acidic fluids can physically fracture the target rock [12] and also dissolve minerals to increase the permeability [13]. Acid

37   fracturing treatment is an effective method to stimulate the production of carbonate reservoirs. However, wormhole

38   propagation induced acid leak-off should be controlled since it is the key to successful acid fracturing [14,15]. Water that

39   returns to the surface after hydraulic fracturing and before production is referred to as flowback water, and the produced

40   water returns from the formation [5]. The water (acid fracturing fluid)-rock interaction involves mineral dissolution, ion

41   exchange, surface complexation and redox reactions, thus leading to the mobilisation of major and trace elements in

42   aqueous environments and resulting in potential environmental and health issues (e.g., Ca, Fe, Mg, As, Cr, Ba, Pb, U, etc)

43   [3,16-19]. Furthermore, the environmental conditions (reservoir temperature and rock/fluid ratio) play an important role

44   in evaluating the water chemistry and environment during water-rock interaction [17]. Unconventional hydrocarbon

45   production by hydraulic fracturing can boost the economy [20], but it may also pose risks to regional water quantity and

46   quality [21-23].

47   The extent of fracture development upon hydraulic fracturing is not well understood and very hard to predict, but

48   the risks of extending fractures into drinking-water aquifers is thought to be very low considering the depth difference of

49   many hundreds of metres or several kilometres between the hydraulic fracturing target and the aquifers [24]. Potential

50   groundwater contamination may result from surface leaks and spills from well pads and wastewater holding ponds, well

51   sealing and integrity failures, and inappropriate wastewater disposal [5,25-27]. Long-term spills and leakages augment

52   environmental risks. Moreover, more than three quarters of spills are likely to contain flowback and produced water, and

53   the geochemical compositions and potential hazardous chemicals in fracturing fluids have raised major concerns [28-30].

54   Therefore, understanding the transport of elements and the composition of fracturing fluids is critical to optimise the

55   treatment and management of both flowback water and produced water, and thus to minimise the impact on the

56   environment.

57   The element mobilisation mechanisms, mobilisation pathways, and mineral morphology during water-rock

58   interaction are discussed in this paper. We conducted three series of five batch reactor experiments under different

59   conditions for two shale samples. These samples cover the end-member mineralogical compositions of basinal shales of

the Bowland-Hodder unit, a Carboniferous deposit in the UK identified as a potential target for unconventional hydrocarbon exploitation [31].

A wide range of fluid acid concentrations, temperatures, and rock/fluid ratios have been tested to investigate element mobilisation and to gain insight into the chemical processes that take place during hydraulic fracturing fluid-shale interaction. Moreover, the alteration in surface morphology of polished shale sample sections by interaction of different minerals with fracturing fluids is discussed, thus enabling a better understanding of the kinetic dissolution of the main minerals. The aim of this paper is thus to gain insight into the mobilisation of elements caused by interaction of Bowland shale with simulated hydraulic fracturing fluids, through quantitative determination of geochemical fluid compositions and physical alteration based on surface topography from batch reactor experiments. Our findings identify the chemical reaction pathways involved and provides new knowledge that may help facilitate defining strategies to mitigate risks regarding potential groundwater contamination related to hydraulic fracturing activities. In terms of future work, we will focus on establishing more quantitative predictive rules on element mobilisation in porous and fractured shale samples, that link shale composition with fluid conditions.

2 Methodology

2.1 Material

The shale samples in this study were collected from the National Geological Repository (NGR) at the British Geological Survey (BGS) in Keyworth. The two samples were taken from the Alston Formation, part of the basinal shales in the Bowland-Hodder Unit [31] of the Roosecote borehole (British National Grid Reference: 323040, 468660) in Cumbria (United Kingdom) from the depths of 618 m (2,027 ft) and 673 m (2,208 ft), and they are referred to in this manuscript as RC618 and RC673, respectively. The Roosecote Borehole was drilled by the Institute of Geological Sciences (IGS, now The British Geological Survey, BGS) in 1970-71 and serves as a stratotype section for the Bowland Shale Formation [32].

The stratigraphically informal 'Bowland-Hodder unit' [31] is based on the seismically defined unit of Fraser et al. [33] consisting of two parts separated by the *Emstites leion* marine band. The upper unit ("Upper Bowland Shale") comprises latest Brigantian – Pendleian (locally Arnsbergian) of post-rift sequences deposited during periodic transgressions in combination with deltaic sequences. The lower unit ("Lower Bowland Shale") consists of syn-rift sediments (Chadian–Brigantian) deposited during the formation of the Pennine Basin (Fig. 1) The Roosecote core was drilled in the northern part of the Craven Basin and samples RC618 and RC673 were taken from the Alston Formation (Lower Bowland Shale, Fig. 1).
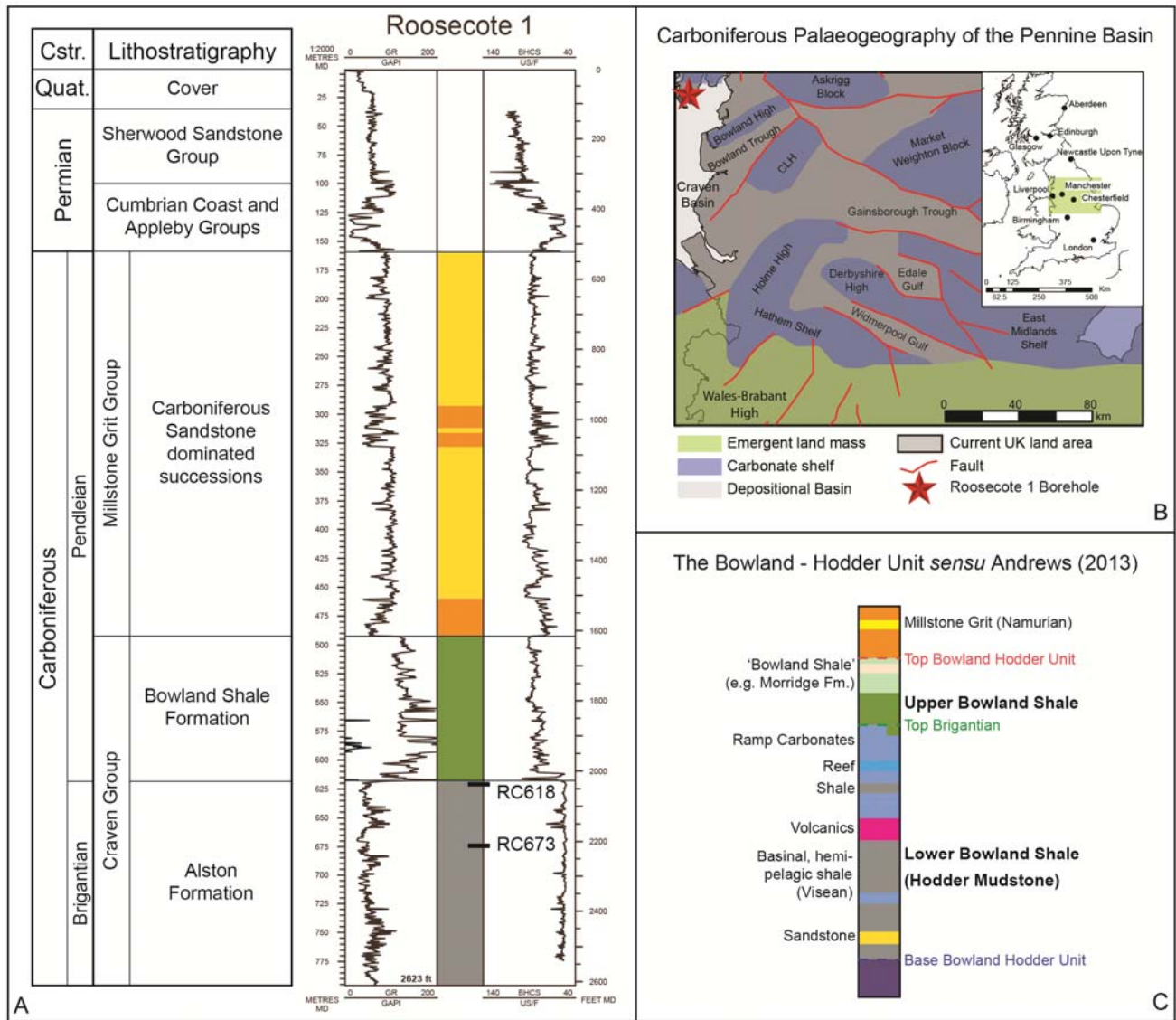
Fig. 1. The Roosecote 1 Borehole. A: chrono- and lithostratigraphy alongside the downhole gamma response [31,34] with indication of sample depths; B: Carboniferous palaeogeography of the Pennine Basin with location of the Roosecote 1 Borehole; C: Idealized cross-section throught the Millstone Grit and Bowland Hodder Unit as a key for the schematic colouring of A (following Hennissen and Gent [35] modification of Andrews [31]). Csrt. = chronostratigraphy, Quat. = Quaternary.

2.2 Sample preparation

For the different series testing experimental parameters, we need ensure the shale sample has the representative mineralogical composition. After drying, grinding (using an agate mortar and pestle), sieving (<125 μm), and mixing, a uniform mineral content can be expected for powdered samples. The powdered samples were used in batch reactor experiments to investigate geochemical element mobilisation by interaction with acidic fluids. Additionally, the powders were used for X-ray diffraction (XRD) analysis to determine their mineralogical composition. Bulk sample powders were scanned over a sampling range of 2.5 to 70 °2θ with a step size of 0.0066 and a scan speed of 0.023 °2θ per second, and a PANalytical X'Pert Pro was applied for these analyses by using Cu K-α radiation at 40 kV and 40 mA. Analysis of the

peak intensities on the sample X-ray diffractograms allow semi-quantitative analysis (using DIFFRAC. EVA-XRD software) for determining of the mineralogical composition (Fig. 2). Moreover, two non-milled pieces of solid shale samples were embedded in epoxy resin, and the sections were finely polished and coated with carbon in preparation for Mineral Liberation Analysis (MLA) and SEM (scanning electron microscope) analysis. During automated MLA-SEM analysis, the Back-Scattered Electron (BSE) signals and Energy Dispersive X-ray spectra (EDS) of the grains are collected. The average BSE grey value of each measurement region relates to a mineral of unique average atomic number, and different mineral components (the mineral identification is based on the chemical composition referenced to a database of minerals) and mineral boundaries can then be identified and established based on the BSE images (Fig. 3) [36]. MLA measurements of different minerals are normalized to 100%. MLA measurements allow the identification of mineralogical components and mineral morphology of the two polished shale samples before and after interaction with acidic fluid. It is noted that the coated carbon was gently removed using diamond powder (after imaging before reaction) before placing the two samples in the acidic solution for chemical reaction. Upon completion of the chemical interaction experiment, carbon was re-applied onto the cross section of the two reacted samples for subsequent MLA measurements. Furthermore, the mineral-surface topography was investigated in these two reacted samples with 3D imaging by using a Zeta-20 Optical Microscope. The focus of the objective lens is moved with Z-stage, and the 3D scanning microscopy of the shale surfaces can be observed by measuring the different vertical heights from the cross section. This information is subsequently used to generate the reconstructed 3D colour images. The optical profiler cannot provide the surface chemical compositions, but the minerals observed by optical microscope can be identified by comparison with the MLA measurements and SEM results. A colour scale is used to represent different heights, the highest height is denoted by the brightest colour, and a lower topography profile is with a darker colour. It seems that the colour represented heights of epoxy resins and quartz are almost the same, and the quartz is therefore selected as a reference in this paper to compare the variations in heights of minerals after acidic treatment (Fig. A.1A and Fig. A.1B).

2.3 Batch reactor experiments

In order to estimate mobilisation of inorganic elements from shale during hydraulic fracturing activities, bench scale batch reactor experiments were conducted to test the interaction of simulated fracturing fluids with the Bowland-Hodder shale at a variety of conditions (a schematic of the experimental apparatus is shown in supplementary material, Fig. A.2), i.e. fluid acidity, temperature, and rock/fluid ratio, as well as two end member mineralogical compositions from the Bowland shale (one with high calcite content, and one with high pyrite and clay content) (Table 1). Hydrochloric acid is the major constituent of fracturing fluid [7,37], and the solution in our experiments was prepared by Milli-Q water, and

the fluid pH was adapted by adding small amounts of concentrated or diluted HCl (trace metal grade). The fluids with stating pH of 2-5 were used to investigate fluid acidity on element mobilisation. Additionally, the fluids with starting pH of 1 were also used to further desorb the metals, thus facilitating the identification of reaction pathways leading to geochemical element mobilisation and maximising the evaluation of the effects of hydraulic fracturing on environmental impacts. The experiments testing the impact of fluid acidity and temperature were conducted at a constant solid to liquid ratio of 1:100 (2 g shale powder in 200 mL solution, which is similar to ratios used in Lavergren et al. [38] and Wang et al. [17]), whereas rock/fluid ratios systematically varied experiments were carried out to evaluate the impacts of changes in rock-fluid contact on elemental mobilisation at a constant fluid pH of 1.0 and ambient temperature of 60 °C (The temperature is selected to simulate the hydraulic fracturing conditions for Bowland shale production in the UK [31], and the experiments are conducted at atmospheric pressure since the geochemical reactions are not really influenced by pressure). In addition, a blank control was conducted (without adding shale particle) and test results demonstrate that element concentration is very close to zero after the interaction of the glass reactor with fracturing fluid (100 h) (Table A.1 and A.2).

Table 1 Summary of experiments (elemental analysis).

| Variable | No. | RC618 | | | | No. | RC673 | | | |
		Starting HCl (mol/L)	Temperature (°C)	rock/fluid ratio (g/mL)	Starting pH		Starting HCl (mol/L)	Temperature (°C)	rock/fluid ratio (g/mL)	Starting pH
fluid acidity	1	10^{-1}	60	2:200	1.1	16	10^{-1}	60	2:200	1.2
	2	10^{-2}	60	2:200	1.9	17	10^{-2}	60	2:200	1.9
	3	10^{-3}	60	2:200	2.7	18	10^{-3}	60	2:200	3.0
	4	10^{-4}	60	2:200	3.6	19	10^{-4}	60	2:200	3.8
	5	Milli-Q water	60	2:200	5.2	20	Milli-Q water	60	2:200	5.1
temperature	6	10^{-1}	25	2:200	1.2	21	10^{-1}	30	2:200	1.0
	7	10^{-1}	30	2:200	1.2	22	10^{-1}	40	2:200	1.0
	8	10^{-1}	40	2:200	1.1	23	10^{-1}	50	2:200	1.2
	9	10^{-1}	50	2:200	1.1	24	10^{-1}	70	2:200	0.9
	10	10^{-1}	70	2:200	1.1	25	10^{-1}	60	20:200	1.1
rock/fluid ratio	11	10^{-1}	60	20:200	1.1	26	10^{-1}	60	4:200	1.0
	12	10^{-1}	60	4:200	1.0	27	10^{-1}	60	0.8:200	1.0
	13	10^{-1}	60	0.8:200	1.0	28	10^{-1}	60	0.4:200	1.0
	14	10^{-1}	60	0.4:200	1.0	29	10^{-1}	60	0.2:200	1.0
	15	10^{-1}	60	0.2:200	1.0					

Each powdered sample was added to a 200 mL solution in a 250 mL closed batch reactor on a hotplate stirrer, where the suspension was continuously stirred using a Teflon-coated magnetic stirrer bar. Each experiment was run for a total of 100 hours, and aliquots (2 mL) were sampled at 0, 1, 3, 7, 23, 27, 31, 54, 77, 100 h and filtered through 0.22 μm polyethersulfone (PES) membranes for further analysis. Hence, the change in pH, as well as the change in geochemical composition of the fluids was recorded over ten time steps in these batch reactor experiments. A total of 1 mL extracted fluid was used for pH analysis by using a Fisher Scientific accumet benchtop pH meter and another 1 mL extracted fluid

was acidified and diluted 10 times with ultrapure HNO_3 (2%) for elemental analysis using inductively coupled plasma optical emission spectroscopy (ICP-OES) and inductively coupled plasma mass spectrometry (ICP-MS), detailed below. The results enable quantification of the extent of geochemical element mobilisation based on the experimental conditions. The results of these experiments, obtained by measuring the elemental concentrations in the fluids, establish the impact of those variables on the effect and rate of leaching, and thus potential contamination. Hence, the data will determine the extent of leaching, mobilisation of elements, and potential contamination by mobilisation of heavy metals.

Furthermore, the surface morphology and topography before and after rock/fluid interaction were observed using two non-milled samples (Table 2).

Table 2 Summary of experiments (MLA and SEM analyses).

No.	Sample	Starting HCl (mol/L)	Temperature (°C)	Starting pH
30	RC618	10^{-1}	60	1.1
31	RC673	10^{-1}	60	1.2

2.4. Analytical techniques of elemental mobilisation

The major elements in our sampled fluids from the batch reactor experiments (Ca, Fe, Al, K, Mg, Na) were quantitatively analysed over ten time steps by ICP-OES. A standard solution (Fisher Chemicals, 100 mg/L) and 2% ultrapure HNO_3 were used to make calibration solutions (0.1, 1, 3, 5, 7, and 10 mg/L). Moreover, ICP-MS is used for trace elemental analysis (Ti, Li, Be, V, Cr, Mn, Co, Ni, Cu, As, Se, Rb, Sr, Mo, Ag, Cd, Cs, Ba, Tl, Pb, U) in the final fluids collected at 100 h. The calibration solutions (20, 40, 100 μg/L) were prepared by using a standard ICP-MS Multi-Element Solution (SPEX CertiPrep) (10 mg/L).

3 Results and Discussion of Major Elements Mobilisation

3.1 Sample characterisation

The XRD results and the semi-quantitative analysis indicate that quartz (61.1%), illite (18.9%), and pyrite (18.0%) are the three main components in the shale sample from 618 m depth (RC618), and calcite (2.0%) is only present at a low abundance (Fig. 2). The shale sample from 673 m depth (RC673) is composed of quartz (88.8%) and calcite (11.2%) (Fig. 2). The results indicate that sample RC618 has a significant content of pyrite and clay (illite), whereas sample RC673 has a noticeable content of calcite.
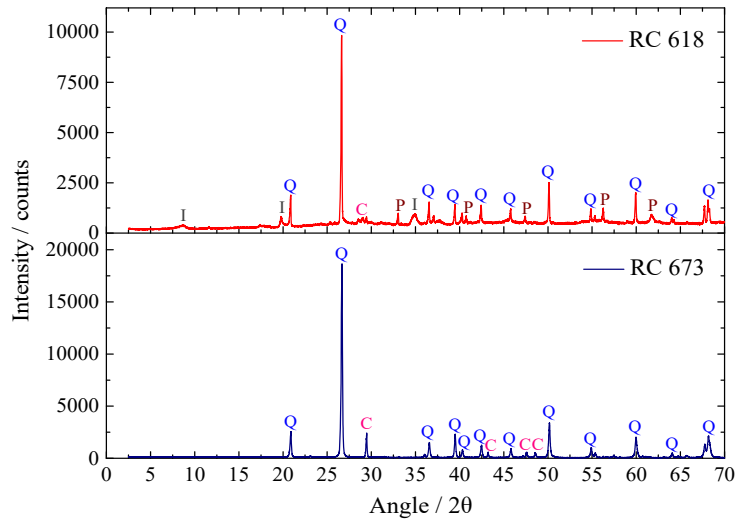
174

Fig. 2. Powder X-Ray Diffractograms: I=illite; Q=quartz; C=calcite; P=pyrite.
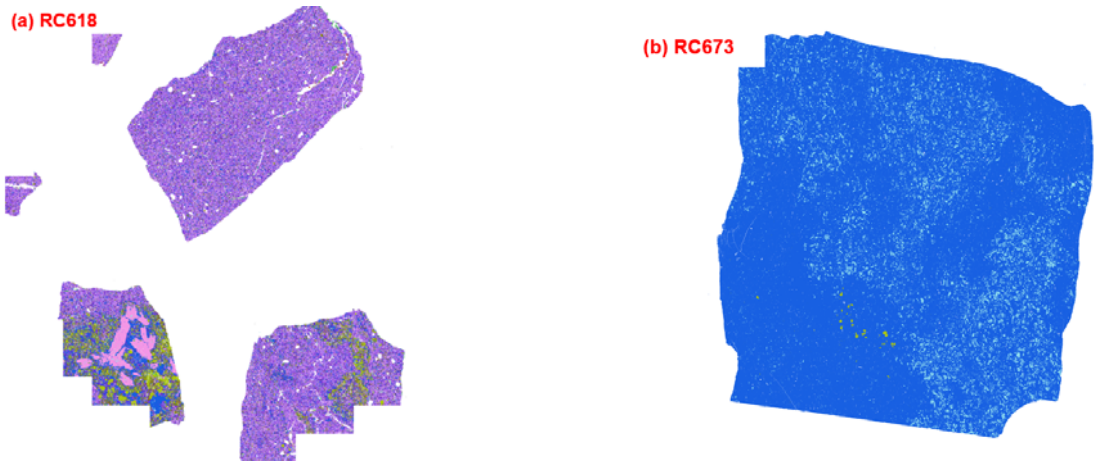
175

Fig. 3. MLA image of shale samples before reaction: (a) MLA measurement of RC618; (b) MLA measurement of RC673.

176

Table 3 MLA data of shale RC618 and RC673 before reaction.

	Mineral	RC618 Formula	Weight	Mineral	RC673 Formula	Weight
	Quartz	SiO_2	13.2%	Quartz	SiO_2	91.1%
	Calcite	$CaCO_3$	0.1%	Calcite	$CaCO_3$	8.7%
	Pyrite	FeS_2	11.2%	Pyrite	FeS_2	0.2%
	Illite	$(K, H_3O)(Al, Mg, Fe)_2(Si, Al)_4O_{10}[(OH)_2, (H_2O)]$	46.6%			
	Barite	$BaSO_4$	5.0%			
	Apatite	$Ca_5(PO_4)_3(F, Cl, OH)$	0.3%			
	Rutile	TiO_2	0.1%			
	Gypsum	$CaSO_4 \cdot 2H_2O$	0.3%			
	Quartz-Illite mix	$SiO_2 \cdot (K, H_3O)(Al, Mg, Fe)_2(Si, Al)_4O_{10}[(OH)_2, (H_2O)]$	15.6%			
	Pyrite-Kaolinite mix	$FeS_2 \cdot Al_2(OH)_4Si_2O_5$	7.6%			
	Diadochite	$Fe_2(PO_4)(SO_4)OH \cdot 5H_2O$	0.1%			

177   The MLA measurement of RC618 shows the heterogeneous distribution of minerals quartz, illite and pyrite (Fig.

8

178   3a; Table 3). The total pyrite content (including mixture with Kaolinite) equals 18.8 weight %, which is very similar to

179   the semi-quantitative XRD result of 18.0%. Moreover, illite and quartz are the main mineral components in RC618,

180   interspersed throughout the sample (Fig. 3a). The MLA measurements for RC673 (Table 3) show that the sample has a

181   lower mineralogical heterogeneity than RC618; it is quartz-rich (91.1 weight %) and has a higher content of calcite (8.7

182   weight %) than RC618, and only a small content of pyrite (0.2 weight %) (Fig. 3b). These MLA results for RC673 are

183   very similar to the XRD measurements. Moreover, uniformly interspersed and widely distributed quartz and calcite have

184   been observed in RC673 (Fig. 3b).

3.2 Variation of pH during fracturing fluid-shale interaction

186   Previous studies have indicated that two of the most reactive minerals in shale include calcite ($CaCO_3$), because of

187   its dissolution in acidic fluids, and pyrite (FeS_2), because of its oxidative dissolution in oxygenated fluids [16-17,39].

188   The pH remains fairly stable or even decreases in experiments with sample RC618 (Fig. 4a and b). Moreover,

189   hydrochloric acid was not added to the fluid in experiment No. 5 (Milli-Q water, starting pH of 5.2), but the fluid pH

190   significantly dropped at the start of the experiment (Fig. A.3A). Subsequently, the fluid acidity stabilized at a low pH,

191   with a value of 2.8 at the end of the experiment (Fig. 4a). This pH behaviour is interpreted to be caused by pyrite oxidative

192   dissolution in RC618, which can lower the fluid pH due to the generation of sulfuric acid (Eqs. 1-3) (e.g. [40]).

193   Additionally, the fluid pH was even stronger in experiments conducted at a higher temperature implying that elevated

194   temperature promotes the oxidative dissolution of pyrite (Fig. 4b). These results are confirmed by the high iron

195   concentrations measured in the fluids, discussed below (Fig. 6). Furthermore, an increased solid to liquid ratio, with

196   higher contents of calcite and clay (e.g. solid to liquid ratio of 20 g: 200 mL, the contents of calcite and illite are 0.4 g

197   and 3.8 g according to XRD data), causes a buffering effect with increase of pH (Fig. 4c).

198   In experiments with RC673, the pH increased rapidly at the start of the experiments, i.e. from 1.9 to 7.1 (Fig. A.4A

199   and Fig. 5a), probably caused by the calcite in the sample which neutralizes the acid (Eq. 4) (e.g. [13,41]). In the

200   experiments with starting fluid pH of 1.0, the amount of calcite in the RC673 sample is not sufficient to neutralise the

201   acid, resulting in a low pH throughout the 100 hours duration of the experiment (Fig. 5b). However, a significantly high

202   solid to liquid ratio contains enough calcite (e.g. 20 g shale sample with RC673 roughly contains 2.2 g calcite) to cause

203   rapid neutralisation of the solution at the start of the reaction (Fig. 5c and Fig. A.4C). Therefore, the acidity- and alkalinity-

204   generating reactions will primarily control the pH of the fracturing fluids, and subsequently affect element mobilisation.
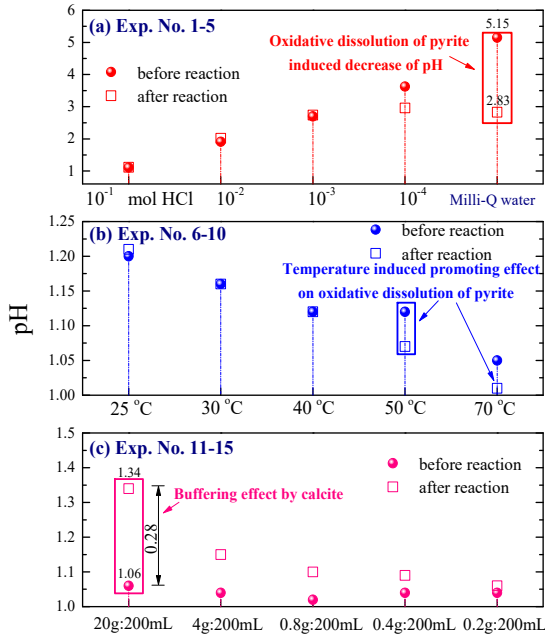
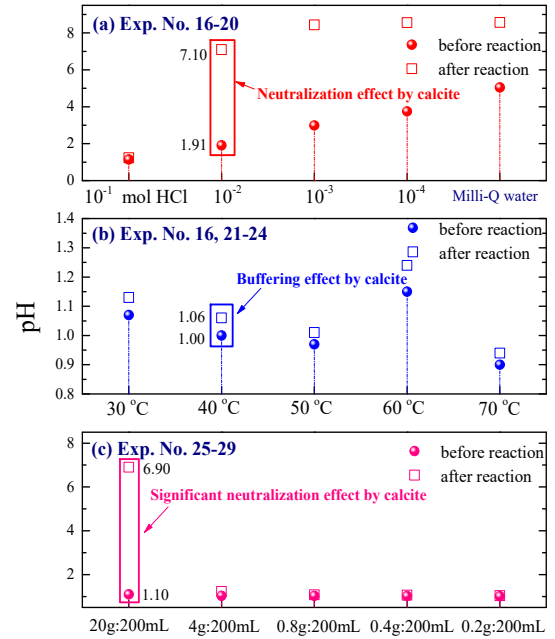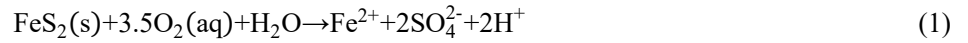**Fig. 4.** pH before and after (100 h) water/rock interaction (RC618).

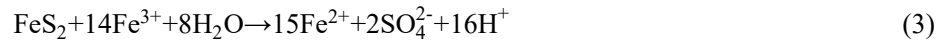**Fig. 5.** pH before and after (100 h) water/rock interaction (RC673).

$$FeS_2(s)+3.5O_2(aq)+H_2O \rightarrow Fe^{2+}+2SO_4^{2-}+2H^+ \tag{1}$$

$$Fe^{2+}+0.25O_2+H^+ \rightarrow Fe^{3+}+0.5H_2O \tag{2}$$

$$FeS_2+14Fe^{3+}+8H_2O \rightarrow 15Fe^{2+}+2SO_4^{2-}+16H^+ \tag{3}$$

$$CaCO_3(s)+2H^+ \rightarrow Ca^{2+}+H_2O+CO_2 \tag{4}$$

3.3 Mobilisation of major elements

3.3.1 Fluid acidity effect

Our experimental results show that fluid acidity has a significant impact on iron (Fig. 6a) and calcium mobilisation (Fig. 7a) in pyrite-rich and calcite-rich rocks, respectively. Harrison et al. [3] consider that the main contributor of dissolved Fe in the experiments is pyrite rather than clays based on the comparison of the dissolution rate of different minerals. The interaction of shale with Milli-Q water (No. 5) showed that the oxidative dissolution of pyrite was the driving force for acid generation [42] and thus increased fluid acidity. It subsequently triggered dissolution of carbonate and clay (e.g. calcite and illite), resulting in the mobilisation of the major elements (Fig. 6a). Furthermore, the solubility of Fe is highly pH-dependent; the precipitation Fe(III)-(oxy)hydroxides commonly occurs in neutral and alkaline environments [43], and thus limits the extent of pyrite dissolution [3] and makes calcite less reactive by the formation of a surface coating [44]. However, there is insufficient calcite in RC618 to buffer the acidity both from the initial fluid and that generated by pyrite oxidative dissolution, thus leading to a low pH (<3) in the fluids (No. 1-5) after reaction (Fig. 4a). The results demonstrate that elevated fluid acidity significantly facilitates the mobilisation of iron, and the Fe concentration increased 131% from 78 mg/L (No. 5, starting pH of 5.2) to 180 mg/L (No. 1, starting pH of 1.1) after 100

10

223   h (Fig. 6a). Williamson and Rimstidt [45] consider that higher pH can lead to faster pyrite dissolution. In order to explain

224   the increased Fe concentration in stronger acid, two possible chemical pathways are presented. First, both Fe^{3+} and O_2

225   are the two most reactive oxidants for pyrite oxidation (Eqs. 1-3) in aqueous solutions, and the pyrite oxidation rate due

226   to the presence of Fe^{3+} is at least two orders of magnitude higher than those due to oxygen dissolved solutions at low

227   pH [46]. Importantly, Wei et al. [47] indicate that Fe-hydroxide precipitates at pH 3.5-4.0. Hence, lower pH reduces iron

228   passivation on pyrite surfaces, increasing ferric ion solubility which acts as the main oxidant that accelerates the

229   dissolution of pyrite. Second, pH driven iron desorption from organic matter at lower pH aqueous solution is also a

230   possible chemical pathway that can raise the Fe concentration [48]. Therefore, we consider that lower fluid acidity will

231   enhance Fe mobilisation in shale, and similar experimental observations have been recorded during the interaction of

232   fracturing fluids with shale [17].

233   The presence of calcium in solution is assigned to the dissolution of calcite, whereas Al, K, and Na are probably

234   derived from interaction with clays (illite) [49]. The leaching of Ca from shale occurs rapidly and stabilizes within 1 h

235   from the start of the reaction, whereas the change in elemental concentration as a function of reaction time indicates an

236   increasing trend for Fe, and to a lesser extent, Al and K concentrations in experiments with RC618 (e.g. Fig. A.5A, A.5B

237   and A.5C). This can be explained by the much faster dissolution of calcite in comparison to aluminosilicates and pyrite

238   [50]. With decreasing fluid acidity, the Ca concentrations remained similar in the different batch experiments (No. 1-5,

239   Fig. 6a), implying that the calcite in RC618 (2.0% according to XRD data) was completely dissolved during reaction

240   because the solutions remained acidic for the entire duration of the reaction. Mg is present in dolomite $(CaMg(CO_3)_2)$

241   and often in clay, and it also commonly substitutes for Ca in calcite [51]. The presence of Mg in our fluids is mainly due

242   to dissolution of aluminosilicate and/or calcite since the MLA and XRD measurements suggest a lack of dolomite in our

243   samples (Fig.3 and Table 3). The increasing Mg concentration (RC618) with increasing fluid acidity suggests that Mg

244   mobilisation probably mainly originates from the dissolution of the clay matrix (illite). The linear correlation between

245   Mg and Al shown in Fig. 8a supports this interpretation.

246   The major cation released from RC673 is calcium (Fig. 7a). The acid concentration has a great impact on calcium

247   mobilisation, with the lowest fluid starting pH (No. 16, 0.1 mol/L HCl) causing the highest Ca concentration (350 mg/L)

248   in solution after 100 h. The experiment with the highest starting pH (No. 20, Milli-Q water) has the lowest Ca

249   concentration (13 mg/L) in solution after reaction (Fig. 7a). The acid concentration significantly affected the extent of

250   calcite dissolution, and the high reactivity of calcite [52] resulted in the rapid release of Ca within 1 h after reaction even

251   in the high rock/fluid ratio (20 g: 200 mL) experiments (Fig. A.6A, A.6B, and A.6C). The rapid dissolution of calcite in

acidic fluids coincides with a rapid pH increase, thus verifying the buffering capacity of calcite [3,50]. Furthermore, the

alkalinity induced metal hydroxide precipitation and higher pH driven adsorption will enable the immobilisation of some

metal ionic species in fracturing fluids [17,53-55] (see section 3.3.3 and 4.3). Increased mobilisation of Mg in RC673

was also triggered by stronger acidic fluids, with the highest Mg concentration (3.3 mg/L) after 100 h in the strongest

acidic fluids, in contrast to 0.4 mg/L Mg after 100 h in the lowest acidity fluid (Fig. 7a). It seems that Mg release is

strongly correlated with Ca mobilisation for RC673. The linear correlation between Mg and Ca (Fig. 8b) indicates that

the release of Mg is mainly derived from calcite dissolution since Mg is commonly incorporated in calcite as an accessory

element [49]. Assuming that all Mg comes from calcite dissolution, 0.94 mol % of Mg (referring to $MgCO_3$) is likely to

be in calcite, and this is a reasonable value for burial calcite in shale (the $MgCO_3$ in Mg-calcite ranges between about

0-32 mol% [56]). A higher Fe concentration is also observed in RC673 at lower fluid acidity (Fig. 7a). The minor

percentage of Al (Fig. 7a) and the significant difference in leaching rate between aluminium and calcium (Fig. A.6A)

suggests that aluminium release is probably derived from minor amounts of clay impurities in the rock matrix and the

results show that increased acidity significantly promoted the mobilisation extent of Al in the fluids.
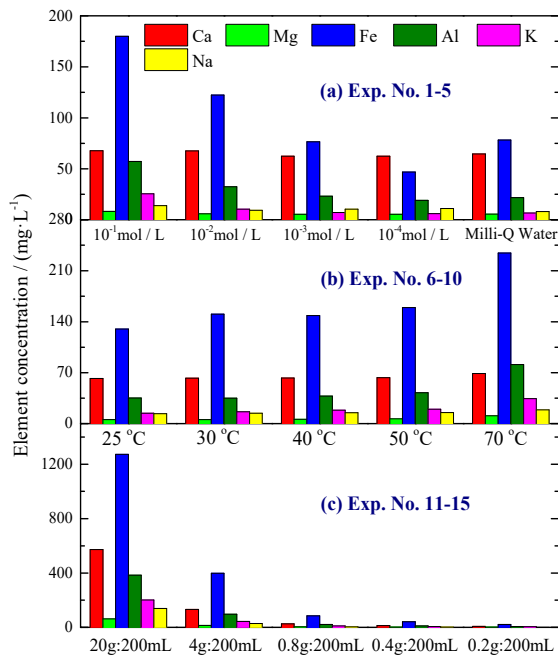
Fig. 6. Elemental composition of the fluids in the experiments with RC618 at different test conditions after 100 hours reaction time.
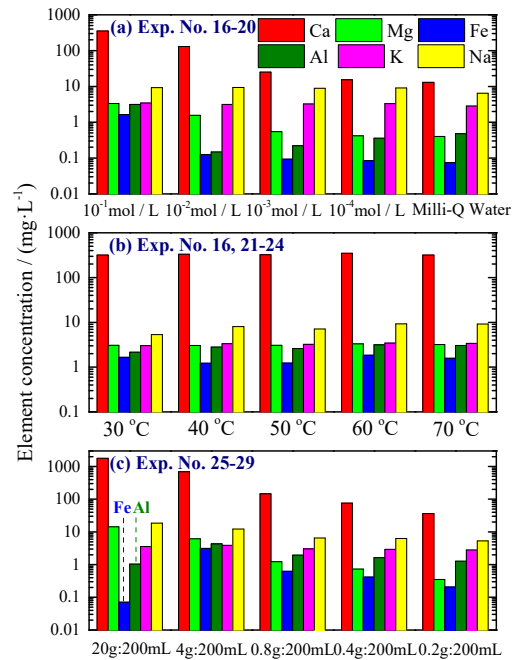

Fig. 7. Elemental composition of the fluids in the experiments with RC673 at different test conditions after 100 hours reaction time.
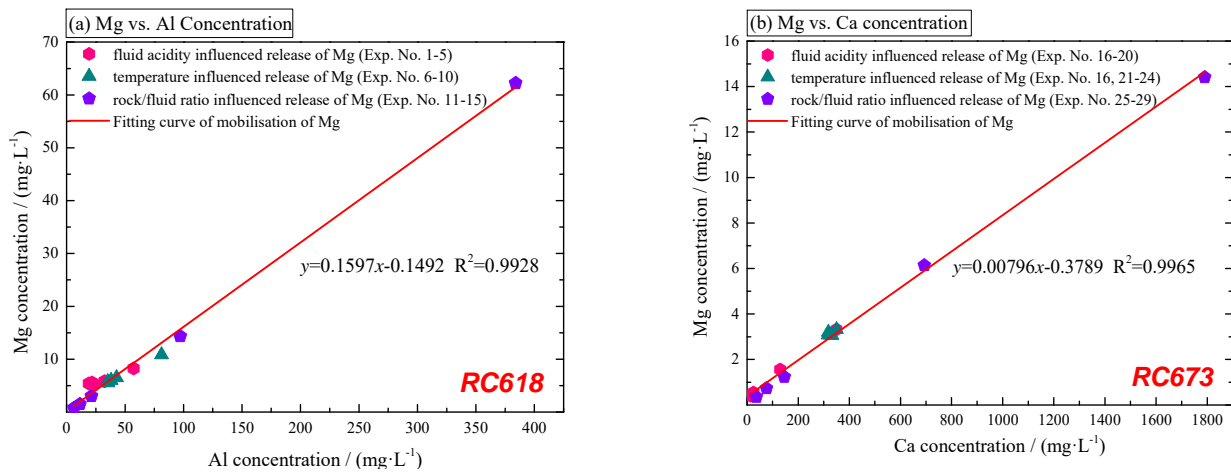
Fig. 8. Mg mobilisation under different experimental scenarios after 100 hours reaction time: (a) Mg vs. Al concentration in RC618; (b) Mg vs. Ca concentration in RC673.

3.3.2 Temperature effect

The experiments aimed at investigating the effect of temperature were conducted with a starting fluid pH of 1.0, and a rock to fluid ratio of 2 g: 200 mL (Table 1). Reactions are commonly faster at higher temperature following the Arrhenius equation [57]. The results indicate a general trend of slightly increased leaching of elements at higher temperature in RC618 samples after a reaction time of 100 h (Fig. 6b), whereas temperature had only little influence on elemental release in experiments with RC673 (Fig. 7b). In the RC618 experiments, the Fe concentration was 129.9 mg/L at 25 °C after 100 h, increasing to 234.5 mg/L at 70 °C. The elevated temperature caused a marked increase in Fe concentration, implying the oxidative dissolution of pyrite was facilitated and accelerated by increased temperature (Fig. 9a). Wang et al. [17] also propose that temperature has a great impact on pyrite oxidation during water-rock interaction. Fe mobilisation in RC673 cannot be detected using ICP-OES since the pyrite content is very low (only 0.2% by MLA measurement), and the data of Fe mobilisation for RC673 was only obtained at the end of our experiments by using ICP-MS with a lower detection limit (Fig. 7b). A similar phenomenon was also observed in the leaching of Al, with Al release in RC618 experiments increasing from 35.3 mg/L to 81.2 mg/L for a temperature increase from 25 °C to 70 °C (Fig. 9b). These results illustrate that the elevated temperature will potentially provide a favourable scenario for the dissolution of aluminosilicate minerals. However, in experiments with RC673, only small differences were observed in calcium (Fig. 9c), as well as magnesium and aluminium release (Fig. A.7A and A.7B). Our experiments show that temperature strongly impacts the oxidative dissolution of pyrite, and to a lesser extent, the dissolution of aluminosilicate. Furthermore, our results demonstrate that the acid concentration (for pH in the range of 1 to 5) influences the dissolution of calcite to a much greater extent than temperature (in the range of 30 to 70 °C).
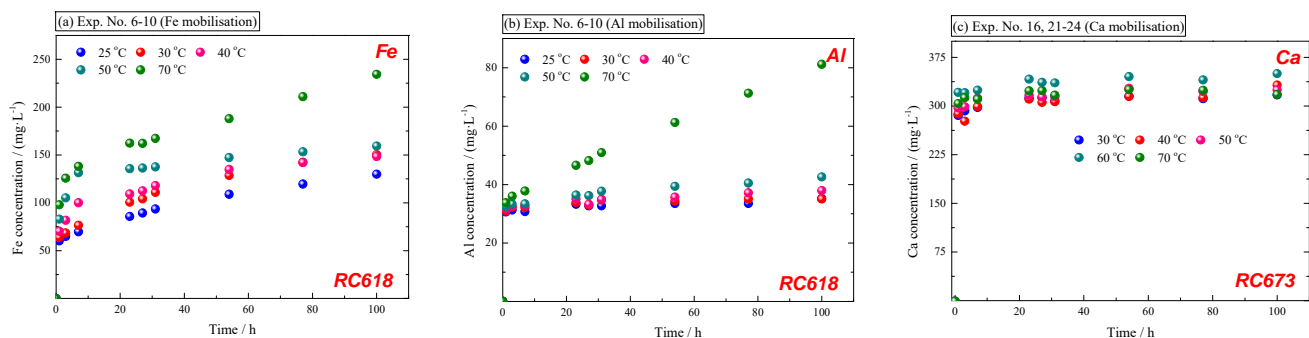
13

Fig. 9. Elemental mobilisation for RC618 and RC673 (0.1 mol/L HCl) at temperatures of 25-70 °C: (a) Fe mobilisation through reaction time; (b) Al mobilisation through reaction time; (c) Ca mobilisation through reaction time.

3.3.3 Rock/fluid ratio effect

The experimental tests conducted to assess the effect of the rock to fluid ratio were conducted at 60 ºC with a starting fluid pH of 1.0. High rock to fluid ratios result in increased contact area between reactive minerals and fracturing fluid. A high rock to fluid ratio strongly facilitates water-rock interaction, and the results show higher element concentrations in the solutions (Fig. 6c and 7c). The Fe concentration in RC618 increased 5905% from 21.2 mg/L (No. 11, 0.2 g: 200 mL) to 1273 mg/L (No. 15, 20 g: 200 mL). Similarly, the concentration of Al increased 5995% from 6.3 mg/L to 384 mg/L. It should be noted that the Fe and Al concentrations do not show a linear correlation. This may be caused by the amount of dissolved calcite (high rock to fluid ratio), which further buffered the solution (Fig. 4c) and decreased the mobilisation of Fe and Al. Interestingly, the Ca concentration in RC618 increased proportionally with the mass of the shale sample after 100 h (Ca concentration increased from 6.9 mg/L to 572 mg/L, Fig. A.8), this is because the fluids maintained a low pH (<1.4, Fig. A.3C) throughout the reaction time, which led to the complete dissolution of the carbonate minerals (e.g. calcite) in the shale.

Higher rock/fluid ratio enables a higher buffering capacity of the shale sample, especially when the content of carbonate minerals is high in the shale formation. The experiments with RC673 show that fluid pH neutralization occurred in the experiment with 20 g shale sample in 200 mL solution with starting fluid pH of 1.0 at 60 ºC (Fig. 5c). The carbonate mineral content increases proportionally with the amount of shale, thus providing enough buffering agent to neutralise the acid. As a consequence, the Ca concentration increases from 36.7 mg/L (for 0.2 g: 200 mL) to 1790 mg/L (for 20 g: 200 mL). Furthermore, the increased contact area between shale and water not only benefited the leaching of calcium but also favoured the mobilisation of Mg, since Mg concentration is strongly dependent on the dissolution of calcite (section 3.3.1). The Mg concentration increases from 0.4 mg/L to 14.4 mg/L with the increase of rock to liquid ratio from 0.2 g: 200 mL to 20 g: 200 mL. In contrast, the concentrations of Fe and Al in RC673 present a different trend, with the highest rock/fluid ratio (20 g: 200 mL, final pH equals to 6.9 at the end of reaction) mobilising the lowest concentration of Fe

14

306 and Al (0.07 and 1.0 mg/L), respectively (Fig. 7c). Since carbonate minerals have a pH buffering effect, the alkalinity

307 generated by the dissolution of calcite may remove some metal ions in aqueous solutions through formation of precipitates

308 at higher fluid pH. The oxidation rate of Fe(II) to Fe(III) increases with increasing fluid pH (e.g. [58]), and subsequent

309 precipitation of Fe-hydroxide is expected. Furthermore, Lee et al. [53] indicate a decreased activity of Al^{3+} at pH>5 is

310 consistent with the formation of solid amorphous $Al(OH)_3$. Seo et al. [59] found that the dissolved Al started to be

311 removed around at pH 4.5 and indicated that most of it was removed at pH 5.5. The fluid pH in the experiment with the

312 highest rock/fluid ratio in this study reached 6.9 after 100 h. Therefore, we consider that this pH environment is favourable

313 for the formation of the hydrolysis product of the Fe- and Al-hydroxides, thus probably resulting in a negative impact on

314 hydrocarbon production by pore blocking. Furthermore, previous studies have shown similar results [3,41,43,55,60].

4 Results and Discussion of Trace Element Mobilisation

4.1 Fluid acidity effects

317   The extent of trace element mobilisation in the RC618 experiments was significantly higher than those of RC673

318 (Fig. 10a and b). The results indicate a general trend of significantly increased release of trace elements at higher acid

319 concentration in RC618 and RC673 experiments after a reaction time of 100 h (Fig. 10a and b). Actually, acid driven

320 forces of solvation deconstruct the mineral lattice and mobilise the trace elements during mineral dissolution. Moreover,

321 lower fluid pH enhances the desorption of metal elements as a result of more H^+ ions competing for adsorption sites on

322 sediment surfaces.

323   Manganese can substitute Ca in the calcite structure [61,62]. The Eh-pH diagram (e.g. [63]) demonstrates that Mn

324 speciation is redox sensitive and pH-dependent. High pH and strong oxidation favours hydrous oxides of Mn^{3+} and

325 Mn^{4+} which are relatively insoluble [59,63]. In RC618 experiments, the fracturing fluids prepared with Milli-Q water

326 and 0.1 mol/L HCl have a final pH of 2.8 and 1.1, and leading to Mn mobilisation of 845 μg/L and 932 μg/L,

327 respectively, after 100 h (Fig. 10a). In addition, the Mn concentration in experiments with RC673 also reached the highest

328 value (312 μg/L) under the strongest acid concentration (0.1 mol/L HCl). However, generated alkalinity by calcite

329 dissolution within higher starting fluid pH (1.9, 3.0, 3.8, and 5.1, No. 17-20) caused rapid neutralisation of the acid after

330 100 h (final fluid pH=7.1, 8.4, 8.6, and 8.6, Fig. 5a) and terminated further Mn release (13.9, 1.6, 1.3, 1.7 μg/L). This

331 behaviour confirmed that Mn mobilisation is very responsive to pH and it is more leachable in a lower pH (acid)

332 environment [49,64], demonstrating that higher pH potentially provides a favourable scenario for Mn oxidation and the

333 formation of poorly soluble Mn-bearing precipitates [47,53,55,59]. Nickel is a siderophilic and chalcophilic element and

334 is a common element in pyrite [42]. The Ni concentration in fracturing fluid slightly increased from 965 μg/L (starting

335 fluid pH of 5.2) to 1004 µg/L (starting fluid pH of 1.1) with the increase of acid concentration (Fig. 10a). Copper was

336 previously documented with a strong association with sulphur (it may be an impurity in pyrite) [65], and Cu can also be

337 adsorbed on the surface of organic matter [48]. Therefore, pH driven mineral dissolution and desorption probably

338 increases Cu concentration (in experiments with RC618) from 349 µg/L (starting fluid pH of 5.2) to 508 µg/L (starting

339 fluid pH of 1.1), and similar elevated concentrations of Cu under strongly acidic conditions were also observed in

340 experiments with RC673 (Fig. 10b). Barium mobilisation may be related to clays such as illite [66]. Our results

341 demonstrate the increased leaching of Ba at low pH (Fig. 10a). Previous studies indicate that Ba release enhanced by

342 acidic conditions may be due to the replacement of adsorbed Ba by a hydrogen ion and the dissolution of some of the

343 coprecipitated hydrous oxides, whilst greater competitive adsorption at exchange sites by other metal ions (e.g. Fe, Mn,

344 and Al) further favour Ba release [67]. The strongest acid concentration (No. 1, starting fluid pH of 1.1) causes the highest

345 mobilisation of Ba (620 µg/L), and the experiment with Milli-Q water has the lowest Ba concentration of 36.6 µg/L

346 after 100 h (Fig. 10a). A similar relationship is noted for Pb, as lower starting pH correlates with a higher Pb concentration

347 after 100 h (Fig. 10a). The strongest acid concentration results in the highest Pb mobilisation of 431 µg/L.
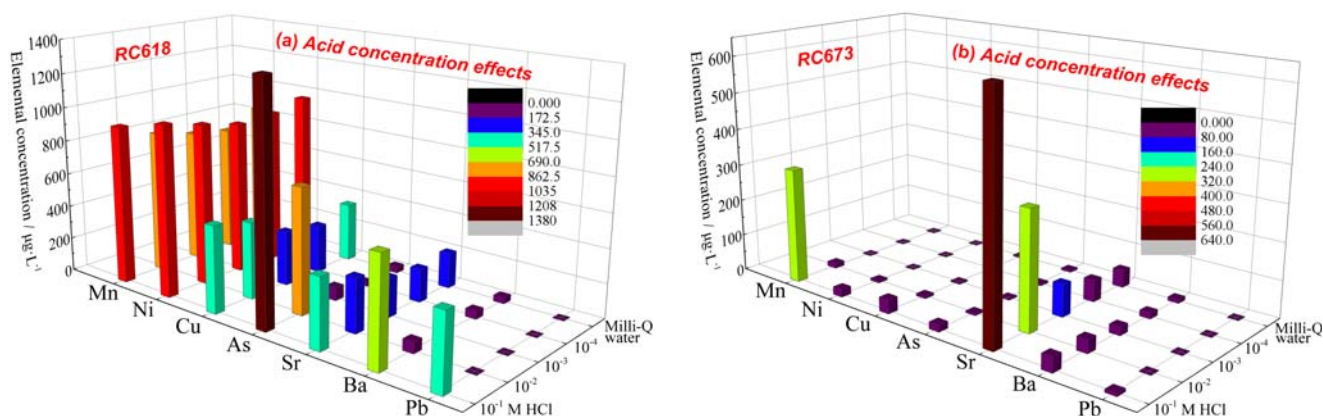

Fig. 10. Trace element mobilisation under different acid concentrations at temperatures of 60 °C with a constant rock/fluid ratio of 2 g: 200 mL: (a) elemental mobilisation in experiments with RC618; (b) elemental mobilisation in experiments with RC673.

348 Furthermore, pyrite can incorporate large amounts of arsenic (up to 10.0 wt %) [68], and the dissolution of pyrite is

349 an important pathway for arsenic mobilisation [69,70]. In experiments with RC618, arsenic was the most abundant trace

350 metal detected in fracturing fluids, the leaching of As is positively correlated with Fe release (Fig. 11a), thus suggesting

351 that As mobilisation is potentially caused by the oxidative dissolution of pyrite. The release of As was significantly

352 influenced by fluid acidity, with the highest As concentration (1376 µg/L) at the strongest acid concentration after 100h.

353 Additionally, in experiments with RC673, strontium was the most abundant trace metal in fracturing fluids, and results

354 indicate that the Sr release was controlled by acid concentration (Fig. 10b). The Sr concentration in fracturing fluids

355 increases with increasing fluid acidity. Harrison et al. [3] suggested the release of Sr was primarily attributed to the

dissolution of carbonate minerals since it is commonly substituted in carbonate minerals [71]. In Luo et al's research [19], a higher concentration of Sr was also found in a higher concentration of Ca aqueous solution. Furthermore, the linear correlation of Sr with Ca demonstrates that the leaching of Sr is likely the result of calcite dissolution (Fig. 11b). Furthermore, it is noted that the concentration of the remaining elements in the experiment is shown in the supplementary material (Fig. A.9-A.11).
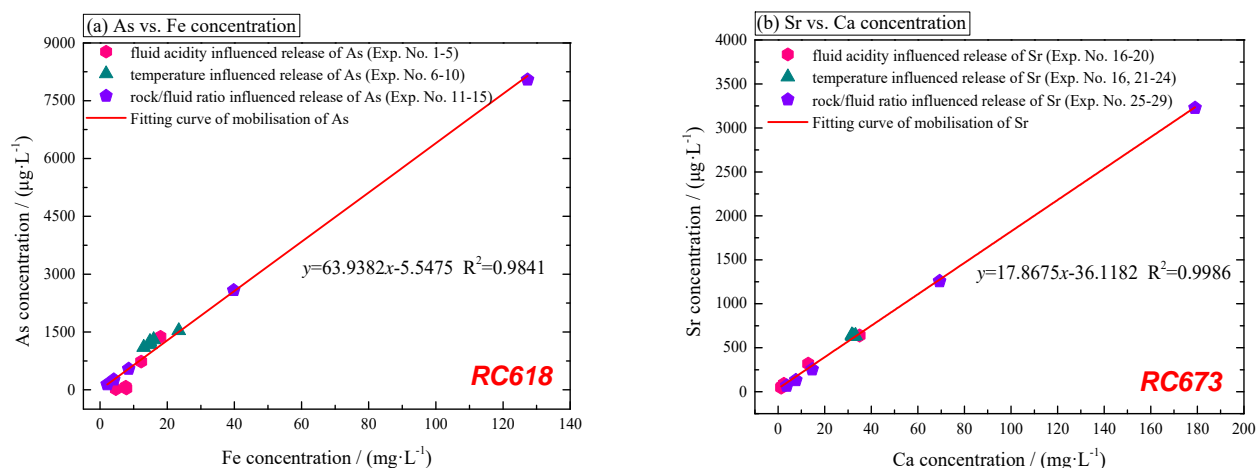
Fig. 11. As and Sr mobilisation under different experimental scenarios after 100 hours reaction time: (a) As vs. Fe concentration in RC618; (b) Sr vs. Ca concentration.

4.2 Temperature effects

Our findings indicate that increased temperature provides a favourable condition for trace element mobilisation in the RC618 experiments, and the mobilisation of the trace elements demonstrates a slight increase with increasing temperature (Fig. 12a). The adsorption of metal ions is generally a spontaneous exothermic process [72]. Therefore, an increase in temperature is unfavourable for adsorption, thereby reducing the adsorption capacity and promoting the leaching of trace elements at exchange sites. Elevated temperature also favours oxidative dissolution of pyrite and dissolution of aluminosilicate minerals (as discussed in section 3.3.2), thereby potentially promoting the mobilisation of some incorporated or substituted trace elements into the fracturing fluids.

Quartz was the main mineral after complete dissolution of calcite in RC673, and temperature influenced the pH of the fluids, from 0.9 to 1.2 after 100 h (Fig. 5). Huang et al. [73] indicate that little measureable adsorption takes place in this acidic pH region since the surface charge of quartz was low. Hence, at this pH scenario, it seems that elevated temperature has little effect on the fate of the trace element including the leaching and fate of accessory trace elements of calcite (Mn and Sr) (Fig. 12b). The maximum difference of Mn concentrations from experiments at different temperatures was 2.4%, and the maximum difference for Sr was 1.7%.
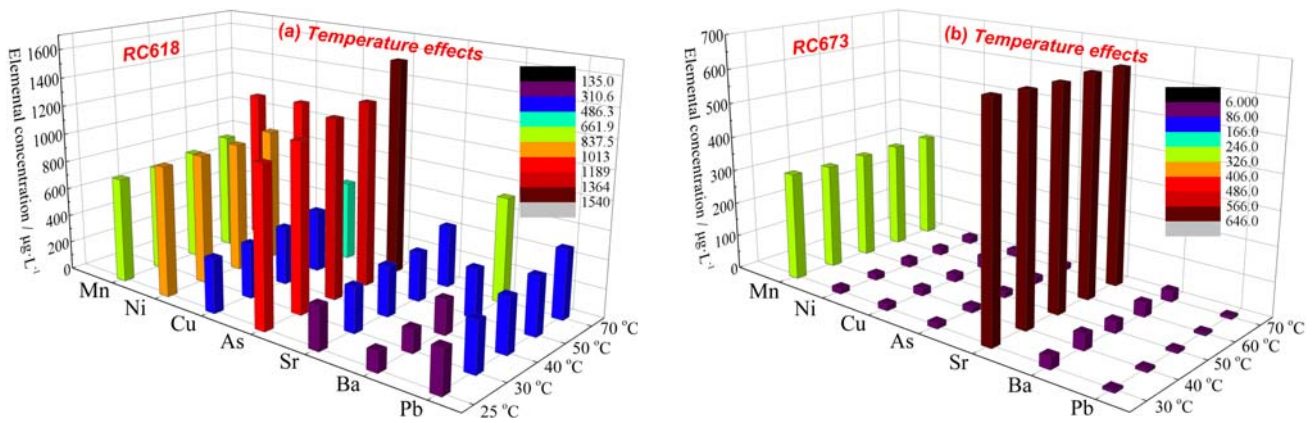
Fig. 12. Trace element mobilisation under different temperatures at acid concentration of 0.1 mol/L HCl with a constant rock/fluid ratio of 2 g: 200 mL: (a) elemental mobilisation in experiments with RC618; (b) elemental mobilisation in experiments with RC673.

4.3 Rock/fluid ratio effect

In RC618 experiments, significant release of Mn, Ni, Cu, As, and Sr (7816, 8813, 3833, 8046, and 2493 μg/L, No. 11) was observed at the rock/fluid ratio of 20 g: 200 mL. The highest release of Mn and Sr in the RC673 experiments was 700 and 3227 μg/L (No. 25). Generally, increased rock/fluid ratio (increased contact area) leads to a relatively higher mobilisation of trace elements from shale (Fig. 13a and b). However, an opposite trend of the mobilisation of Ba and Pb was observed (Fig. 13a), whereby the highest rock/fluid ratio results in the lowest concentration of barium (68.9 μg/L) and lead (7.9 μg/L). It should be noted that illite is usually negatively charged mainly due to the tetrahedral isomorphic substitution of Si^{4+} by Al^{3+} [74], and the migration of positively charged metal ionic species will therefore be affected through electrostatic interactions. If there are less H^+ ions available in the fracturing fluids, this benefits adsorption of heavy metals because of competitive adsorption of hydrogen ions and metal ions, and further elevated pH may induce the precipitation of metal ions by the formation of metal hydroxides. Therefore, the mobility of different metal ions is significantly affected by the hydration of elements and the surface properties of clay minerals [75]. Actually, the mobility of barium is limited in clays due to a strong cation exchange selectivity for Ba [76-78], and higher pH (Fig. 4c) favours the adsorption of Ba onto clay surface as a result of less H^+ ions competing for adsorption sites on mineral surfaces. Hence, higher fluid pH observed at higher rock/fluid ratio (section 3.2) results in decreased Ba concentration in the fluids. Furthermore, sulphate is generated in fluids during the ongoing oxidative dissolution of pyrite, and the precipitation of barite is also a possible pathway that can decrease the Ba concentration [17]. The release of Pb is potentially restricted by adsorption at the surface of and/or co-precipitation with iron and manganese oxides [3,49,79]. Moreover, He et al. [74] found and proposed that Pb^{2+} shows a strong affinity for illite based on their adsorption experiments at varying pH since the ion radius of Pb^{2+} (1.32 Å) is very similar to that of K^+ (1.33 Å), and the

mobilisation of Pb in our study at the highest rock/fluid ratio also confirms the affinity of Pb to illite (Fig. 13a). A higher rock/fluid ratio leads to higher pH and potentially causes more negative surface charges. Hence, both higher fluid pH and similar ionic radius between Pb^{2+} and K^+ will provide a favourable scenario for the replacement of K^+ by Pb^{2+} in the interlayer of illite. Our results illustrate that higher rock/fluid ratios will potentially immobilise some cations through adsorption.

The highest rock/fluid ratio of 20 g: 200 mL in the RC673 experiments provided enough calcite to neutralise the acid (pH 6.9), whereas the fluid pH was below 1.3 for a lower rock mass ($\leq$4 g) in the experiments (Fig. 5c). As discussed in section 4.1, to some extent, Sr release could indicate the dissolution extent of calcite, and thus more Sr is released in the experiment with higher rock/fluid ratios (Fig. 13b). The Sr concentration in the fluids continuously increased from 67.3 (0.2 g: 200 mL, No. 29) to 3226.8 µg/L (20 g: 200 mL, No. 25). The Mn concentrations released by 20 g shale (700 µg/L) and 4 g shale (622 µg/L) in the fluid were not much different (Fig. 13b), and this was probably due to the higher pH conditions that are favourable for Mn oxidation as discussed in section 4.1.
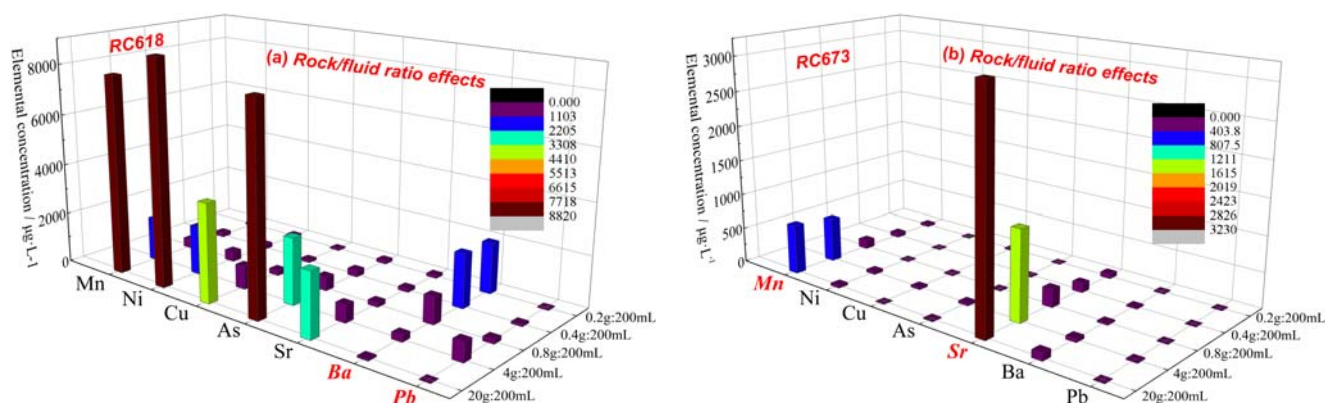

Fig. 13. Trace element mobilisation at different rock/fluid ratios, temperature of 60 °C and acid concentration of 0.1 mol/L HCl: (a) elemental mobilisation in experiments with RC618; (b) elemental mobilisation in experiments with RC673.

5 Morphology and topography of minerals after interaction with acidic fracturing fluids

5.1 MLA/SEM analysis of the surface morphology after treatment with acidic fluids

The MLA measurements can be used to make an evaluation of mineral distribution before and after reaction. The two solid samples were exposed to 200 mL acidic fluids (0.1 mol/L HCl) at a temperature of 60 °C. In the experiments with RC618 and RC673, the starting fluid pH was 1.1 and 1.2, respectively. After 100 h rock/fluid interaction, the fluid pH was 1.1 for both. Hence, almost no change in fluid pH, in contrast to some results from the experiments with shale powder, which can be explained by the difference in sample surface area.

After exposure to the acidic fluids, a large amount of secondary fractures on the shale surface (RC618) were observed (Fig. 14a), in comparison with the MLA measurement before reaction (Fig. 3a). Previous studies indicated that

clay hydration by water intake always produces water-induced fractures in shale [80,81], and these secondary fractures probably enhance the total rock permeability [82]. Clay minerals are hydrophilic, and Wang et al. [83] indicated that spontaneous imbibition of water is caused by the capillary effect (dominated by micro cracks and pores), and subsequent clay hydration induced internal stresses [84] will initiate micro cracks and affect the structural integrity (including mechanical properties) of the shale. The mineral composition (Table 4) exhibits the fully dissolved calcite, whereas the variations in illite and pyrite were not significant. This is probably due to different mineral dissolution kinetics as discussed in section 3.3.1.

Complete dissolution of calcite (Table 4) on the polished surface of shale RC673 was observed after interaction with acidic fluid (Fig. 14b). Clear and widely distributed dissolution pores were left after dissolution of calcite (Fig. 14b). These dissolution pores can potentially provide large amounts of nucleation points to trigger further formation and propagation of cracks in shale reservoirs [85], thus maximising the formation of fracture networks.
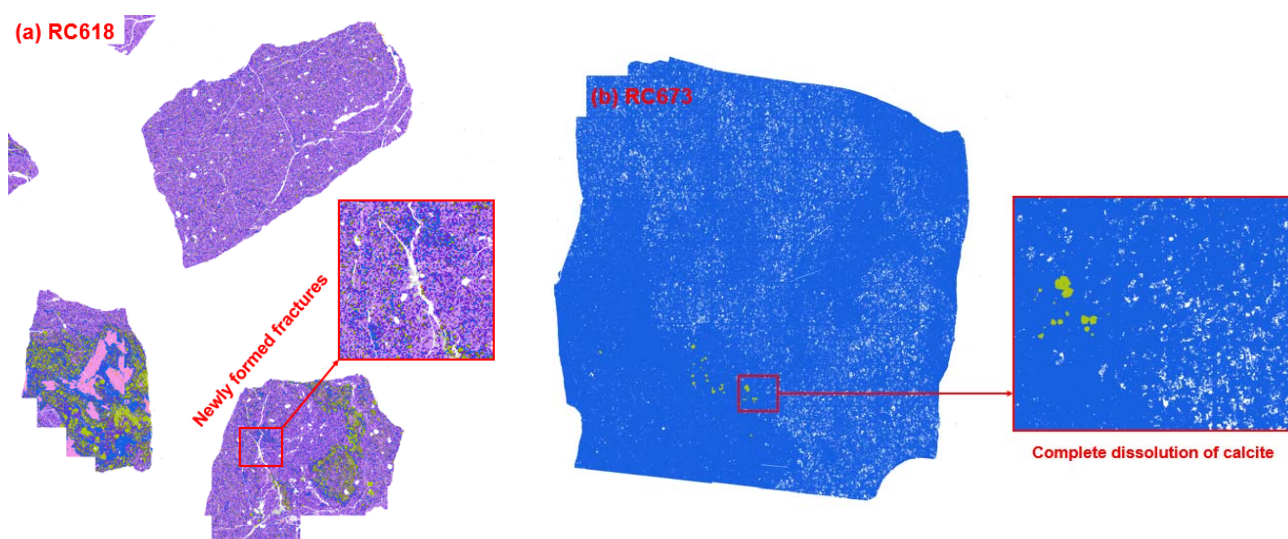

Fig. 14. MLA image of shale samples after reaction: (a) MLA measurement of RC618; (b) MLA measurement of RC673.

Table 4 MLA data of shale RC618 and RC673 after reaction.

		RC618			RC673	
	Mineral	Formula	Weight	Mineral	Formula	Weight
	Quartz	SiO_2	14.4%	Quartz	SiO_2	99.8%
	Calcite	$CaCO_3$	0.0%	Calcite	$CaCO_3$	0.0%
	Pyrite	FeS_2	11.5%	Pyrite	FeS_2	0.2%
	Illite	$(K, H_3O)(Al, Mg, Fe)_2$ $(Si, Al)_4O_{10}[(OH)_2, (H_2O)]$	44.8%			
	Barite	$BaSO_4$	4.5%			
	Apatite	$Ca_5(PO_4)_3(F, Cl, OH)$	0.01%			
	Rutile	TiO_2	0.1%			
	Gypsum	$CaSO_4 \cdot 2H_2O$	0.0%			
	Quartz-Illite mix	$SiO_2 \cdot (K, H_3O)(Al, Mg, Fe)_2$	17.4%			

20

		$(Si, Al)_4O_{10}[(OH)_2, (H_2O)]$	
■	Pyrite-Kaolinite mix	$FeS_2 \cdot Al_2(OH)_4Si_2O_5$	7.3%
■	Diadochite	$Fe_2(PO_4)(SO_4)OH \cdot 5H_2O$	0.0%

427 SEM images of shale RC618 were taken to analyse mineral morphology before and after reaction. Pyrite crystals

428 found in shale RC618 have several shape characteristic of aggregate, nodular and irregular (Fig. 15a-d), which are similar

429 to the classification of pyrite grains by Yoshiya et al. [86]. Although the difference in pyrite grains cannot be observed by

430 SEM images, the dissolution of pyrite grains was confirmed by the surface topography of pyrite (see section 5.2). The

431 newly formed fracture due to clay hydration can be observed (Fig. 15d), which is similar to the fracture demonstrated in

432 Fig. 14a. Hydration of clay weakens the cementation between particles and decreases the internal friction angle and

433 compressive strength, and hydration stress by water adsorption will further facilitate the formation of micro-cracks in

434 shale [83].

435 Calcite is widely distributed in shale RC673, the SEM images demonstrate the complete dissolution of calcite after

436 interaction with acidic fluid. This altered the surface morphology of the polished shale sample, and well-developed micro-

437 fractures can then be identified (Fig. 15f and h). A very small amount of pyrite grains (Table 4) showed local abundance,

438 and the distributed pyrite grains can still be detected on the shale surface after 100 h reaction with acidic fluid (Fig. 15h).

439 The main shape characteristics of pyrite grains were hexagonal and aggregate in shale RC673 (Fig. 15h). The preferential

440 dissolution of calcite (Fig. 15f and h) implies that calcite grains are much more reactive than pyrite grains in acidic

441 solutions, thus rapidly enhancing the porosity of the shale. The difference in the surface morphology of calcite and pyrite

442 grains confirms a faster release of calcium, and this also suggests that Sr could be rapidly mobilised at the initiation and

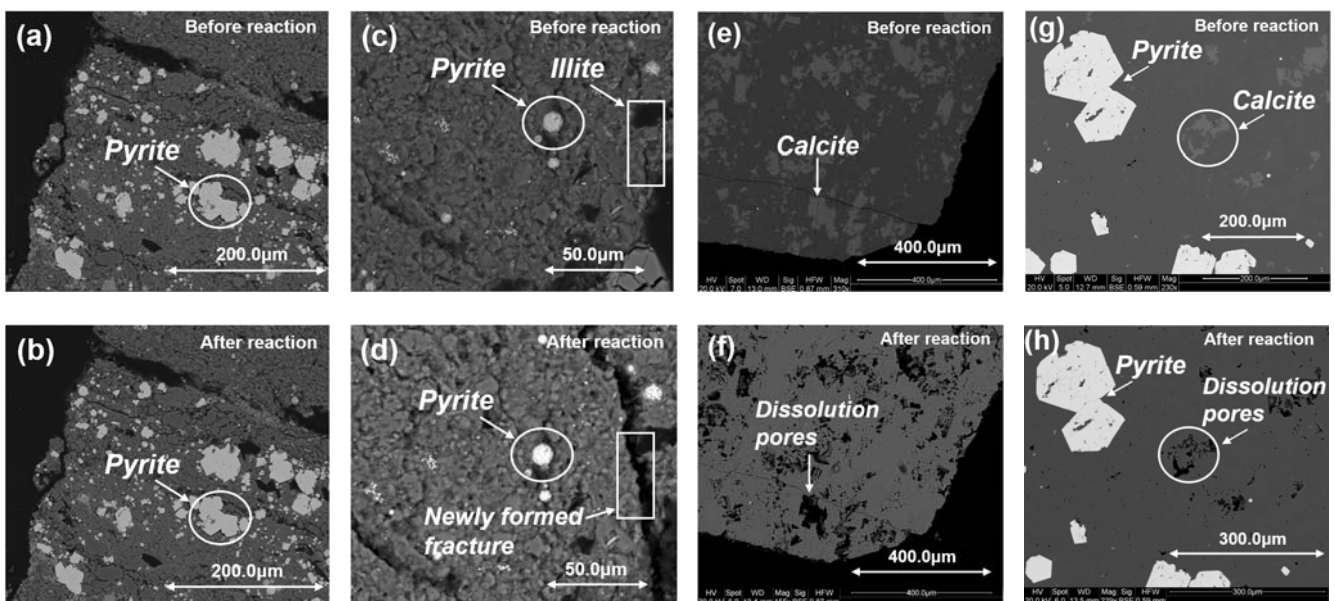443 early stage of fracturing activities.

Fig. 15. SEM images of the different minerals morphology before and after reaction (100 h) with acidic fluid: (a-d) SEM images of RC618; (e-h) SEM images of RC673.

5.2 Surface topography of minerals after treatment with acidic fluids

Analysis of topographical features on sectioned shales will help to investigate the alteration in surface morphology and porosity. A 3D optical profiler (Zeta-20 Optical Microscope) was used to examine the topography of the shale polished surfaces and heterogeneity of surface minerals after reaction with acidic fluids. The complete dissolution of calcite can be observed by using the 2D image (Fig. A.1A), whereas the dissolution pores appeared in the form of noise in the 3D images (Fig. A.1B). This may happen if the local slope of the dissolution pore (left by dissolved calcite) exceeds the allowed maximum slope since the reflected light will be sent outside the objective of the microscope.

It seems that the internal structure damage (spalling of illite) in shale RC618 results in a rougher surface (Fig. 16a-c) compared to the surface of shale RC673, which consists mainly of quartz (Fig. 16d). This is due to the water adsorption by clay-rich shale that can generate local internal stress and thus cause spalling and induce fractures [80,84]. The regions of porosities left by the collapse of clay will increase the contact area between pyrite and the acidic fluid, and probably enhancing further oxidative dissolution of pyrite. The pyrite grains observed in Fig. 16a correspond to the pyrite grains shown in Fig. 15b, the height of pyrite was significantly higher than that of illite. Different surface heights of pyrite and quartz (Fig. 16a-d) illustrate that the position of the aggregate and hexagonal pyrite grains are lower, which means that pyrite grains are more dissolved. The Fe concentration due to pyrite dissolution by shale RC618 and RC673 in the fluids was 28.4 mg/L and 0.1 mg/L after 100 h reaction (approximately 1.1 and 4.1×10^{-3} mm^3 of pyrite have been dissolved), respectively (No. 30 and 31, Table A.3). A hexagonal pore structure formed after the dissolution of hexagonal pyrite grains, to some extent, suggesting the mineral shape will influence the pore geometry (Fig. 16d). Therefore, the mineralogical compositions, and the shape and spatial distribution of reactive minerals may play an important role in determining the pore geometry and pore network after rock/fluid reaction. Furthermore, calcite dissolves faster than pyrite since both pyrite and calcite grains were in the same water environment (Fig. 16d). This confirms a faster kinetic dissolution of calcite [50], and it is also consistent with the rapid mobilisation of calcium as observed in section 3.3.1.
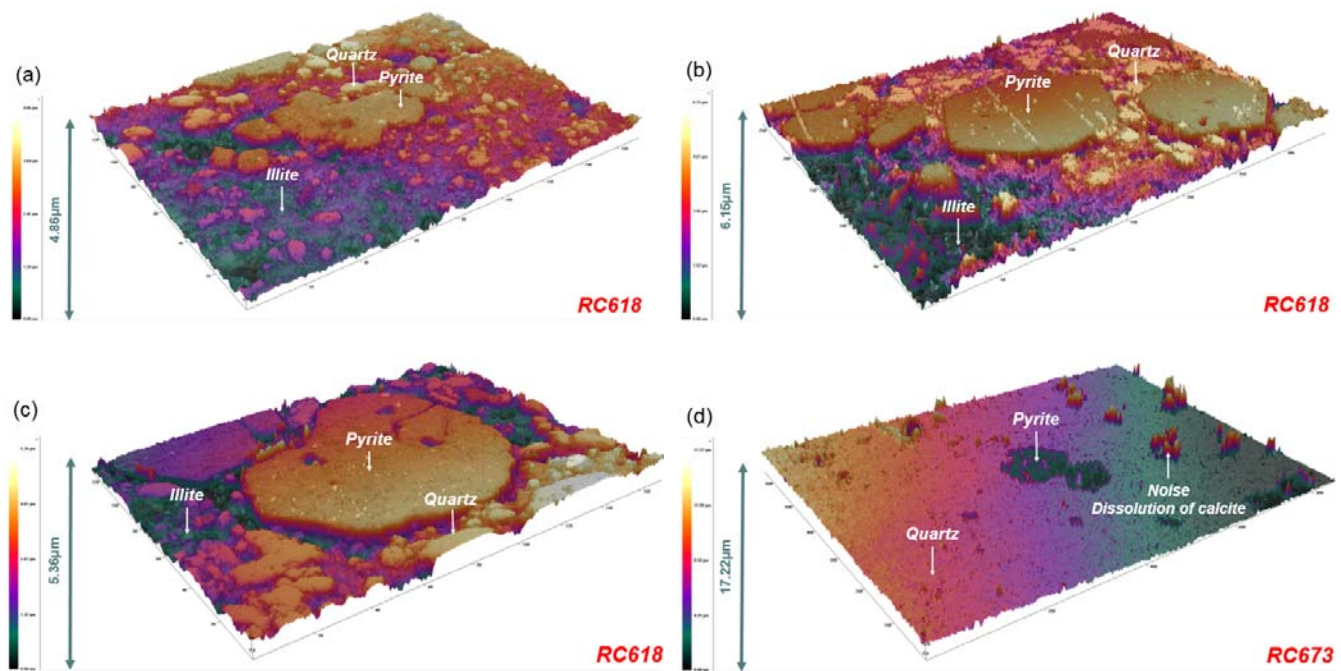
Fig. 16. 3D colour surface profiles of different minerals after acidic treatment in shale RC618 and RC673.

Conclusions

Several series of batch reactor experiments were carried out to determine elemental mobilisation from simulated fracturing fluids over a range of fluid chemistries and other conditions. The underlying chemical mechanisms behind element mobilisation involve mineral dissolution and element desorption at interfacial contacts, and strongly dictate the chemistry of flowback water. Moreover, the morphology and topography of the altered zone in the shale matrix (Carboniferous Bowland-Hodder unit, UK) enable a better understanding of pore generation and the kinetic dissolution of the main minerals during water-rock interaction. Our main conclusions are:

(1) The oxidative dissolution of pyrite can lower the fluid pH, and authigenous calcite in the shale acts as a buffering agent since it dissolves due to reaction with the acid. The acidity- and alkalinity-generating reactions will primarily balance the pH of the fracturing fluids, and subsequently affect the geochemical composition of the fracturing fluids.

(2) Elevated fluid acidity has a major influence on element mobilisation as in general, a low pH significantly favours the mobilisation of major elements (Ca, Mg, Fe, Al, K, Na). Calcite is found as the most reactive mineral amongst the main minerals observed in the shale samples; the leaching of Ca from shale occurs rapidly and stabilizes shortly after the initiation of the reaction. In contrast, the Fe release originating from the dissolution of pyrite demonstrates an increasing trend with time, and to a lesser extent, the mobilisation of Al and K, as well, derived from illite.

A higher acid concentration favours the mobilisation of trace elements (Mn, Ni, Cu, As, Sr, Ba, Pb) through mineral dissolution and pH-driven desorption. The release of As and Sr is positively correlated with the mobilisation of Fe and

483 Ca, respectively, suggesting that the leaching of As and Sr is likely originated from the dissolution of pyrite and calcite,

484 respectively.

485   (3) An increase in temperature enhances oxidative dissolution of pyrite, and to a lesser extent, dissolution of

486 aluminosilicates. Our results demonstrate that the acid concentration (for pH in the range of 1 to 5) influences the

487 dissolution of calcite to a much greater extent than temperature (in the range of 30 to 70 ºC). The extent of calcite

488 dissolution in this temperature range is about the same, thus the difference in the release of its accessory element of Mn

489 and Sr is small. In addition, it seems that a higher temperature favours desorption, thereby reducing the adsorption

490 capacities and promoting the leaching of trace elements at the exchange sites.

491   (4) Higher rock/fluid ratio increases water-rock contact, which results in a higher concentration of most elements

492 released in the simulated fracturing fluid. However, high rock/fluid ratio (elevated mass of carbonate minerals) also

493 increases the capacity to generate alkalinity, which could possibly accelerate the adsorption of some trace metals because

494 of decreased competition for exchangeable sites (e.g. Ba and Pb). Furthermore, the alkalinity generation (pH increase)

495 can probably provide a favourable scenario for the immobilisation and removal of some metal ions through the formation

496 of hydrolysis products (e.g. Fe-, Al-hydroxides) and oxidative precipitation (e.g. Mn oxides).

497   (5) The newly formed macroscopic fractures after water-rock interaction are probably due to the generated local

498 internal stresses during clay hydration. The mineralogical composition and the shape and spatial distribution of reactive

499 minerals potentially play an important role in determining the pore geometry and pore network after water-rock

500 interaction. The mineral topography demonstrates the preferential dissolution of calcite, related to the rapid mobilisation

501 of calcium. Moreover, the dissolution pores may act as nucleation points for crack formation.

502   (6) The contaminants released in drinking water is a major health concern, and the World Health Organization (WHO)

503 has proposed guideline value for drinking water. Elements such as Pb, Mn, Ba and As have concentration guidelines in

504 waters (10 μg/L, 0.4 mg/L, 1.3 mg/L, and 10 μg/L, respectively) [87]. Therefore, their mobilisation is an important

505 observation.

References

[1] Yuan J, Luo D, Feng L. A review of the technical and economic evaluation techniques for shale gas development. Appl Energy 2015;148:49-65.

[2] Myers T. Potential contaminant pathways from hydraulically fractured shale to aquifers. Ground Water 2012;50(6):872-82.

[3] Harrison AL, Jew AD, Dustin MK, Thomas DL, Joe-Wong CM, Bargar JR, Johnson N, Jr GEB, Maher K. Element release and reaction-induced porosity alteration during shale-hydraulic fracturing fluid interactions. Appl Geochem 2017;82:47-62.

[4] Li Y, Yang S, Liu D, Yang C, Yang Z, Li H, Tang Z. Experimental study of shale-fluids interaction during oxidative dissolution with hydrogen peroxide, sodium hypochlorite and sodium persulfate. Appl Geochem 2020;113:104503.

[5] Vidic RD, Brantley SL, Vandenbossche JM, Yoxtheimer D, Abad JD. Impact of Shale Gas Development on Regional Water Quality. Science 2013;340(6134):1235009.

[6] Kumari WGP, Ranjith PG, Perera, MSA, Li X, Li LH, Chen BK, Avanthi Isaka BL, De Silva VRS. Hydraulic fracturing under high temperature and pressure conditions with micro CT applications: Geothermal energy from hot dry rocks. Fuel 2018;230:138-54.

[7] Gregory KB, Vidic RD, Dzombak DA. Water management challenges associated with the production of shale gas by hydraulic fracturing. Elements 2011;7:181-6.

[8] Council of Canadian Academies. Environmental impacts of shale gas extraction in Canada. Ottawa, ON: the expert panel on harnessing science and technology to understand the environmental impacts of shale gas extraction, Council of Canadian Academies 2014.

[9] King GE. Hydraulic Fracturing 101: What Every Representative, Environmentalists, Regulator, Reporter, Investor, University Researcher, Neighbor and Engineer Should Know About Estimating Frac Risk and Improving Frac Performance in Unconventional Gas and Oil Wells. Paper presented at SPE Hydraulic Fracturing Technology Conference, The Woodlands, Texas 2012.

[10] Guo T, Li Y, Ding Y, Qu Z, Gai N, Rui Z. Evaluation of acid fracturing treatments in shale formation. Energy Fuels 2017;31:10479-89.

[11] Hou B, Zhang R, Chen M, Kao J, Liu X. Investigation on acid fracturing treatment in limestone formation based on true tri-axial experiment. Fuel 2019;235:473-84.

[12] Cheng Y, Lu Y, Ge Z, Cheng L, Zheng J, Zhang W. Experimental study on crack propagation control and mechanism analysis of directional hydraulic fracturing. Fuel 2018;218:316-24.

[13] Morsy S, Sheng JJ, Hetherington CJ, Soliman MY, Ezewu RO. Impact of matrix acidizing on shale formations. In: Paper SPE 167568 Presented at the Nigeria Annual International Conference and Exhibition Held in Lagos, Nigeria, 2013.

[14] McCartney E, Al-Othman M, Alam A, Nino-Penaloza A, Pirogov A, Nagarkoti M, Mendez A. Enhanced acid fracturing with improved fluid loss control and near wellbore diversion increases production in Kuwait. In: SPE AnnualTechnical Conference and Exhibition. Society of Petroleum Engineers, 2017.

545 [15] Zhang Y, Yang S, Zhang S, Mou J. Wormhole propagation behavior and its effect on acid leakoff under in situ conditions in acid fracturing.

546   Transp Porous Med 2014;101:99-114.

547 [16] Wilke FDH, Vieth-Hillebrand A, Naumann R, Erzinger J, Horsfield B. Induced mobility of inorganic and organic solutes from black

548   shales using water extraction: Implication for shale gas exploitation. Appl Geochem 2015;63:158-68.

549 [17] Wang L, Burns S, Giammar DE, Fortner JD. Element mobilization from Bakken shales as a function of water chemistry. Chemosphere

550   2016;149:286-93.

551 [18] Wang K, Xu T, Wang F, Tian H. Experimental study of CO_2-brine-rock interaction during CO_2 sequestration in deep coal seams. Int J

552   Coal Geol 2016;154-155:265-74.

553 [19] Luo X, Ren X, Wang S. Supercritical CO_2-water-shale interactions and their effects on element mobilization and shale pore structure

554   during stimulation. Int J Coal Geol 2019;202:109-27.

555 [20] Jarvie DM. Shale resource systems for oil and gas: part 1-shale-gas resource systems. In: Breyer, J. A. (Ed.), Shale Reservoirs-Giant

556   Resources for the 21st Century, AAPG Memoir. Am Assoc Pet Geol 2012;97:69-87.

557 [21] Estrada JM, Bhamidimarri R. A review of the issues and treatment options for wastewater from shale gas extraction by hydraulic

558   fracturing. Fuel 2016;182:292-303.

559 [22] Torres L, Yadav OP, Khan E. A review on risk assessment techniques for hydraulic fracturing water and produced water management

560   implemented in onshore unconventional oil and gas production. Sci Total Environ 2015;539:478-93.

561 [23] Liu D, Li J, Zou C, Cui H, Ni Y, Liu J, Wu W, Zhang L, Coyte R, Kondash A, Vengosh A. Recycling flowback water for hydraulic

562   fracturing in Sichuan Basin, China: Implications for gas production, water footprint, and water quality of regenerated flowback water.

563   Fuel 2020;272:117621.

564 [24] Mair R, Bickle M, Goodman D, Koppelman B, Roberts J, Selley R, Shipton Z, Thomas H, Walker A, Woods E, Younger P. Shale gas

565   extraction in the UK: a review of hydraulic fracturing. London: Royal Academy of Engineering 2012.

566 [25] Davies RJ, Almond S, Ward RS, Jackson RB, Adam C, Worrall F, Herringshaw LG, Gluyas JG, Whitehead MA. Oil and gas well and

567   their integrity: Implication for shale and unconventional resource exploitation. Mar Petrol Geol 2014;56:239-54.

568 [26] Jackson RB, Vengosh A, Carey JW, Davies RJ, Darrah TH, O'Sullivan F, Pétron G. The environmental costs and benefits of fracking.

569   Annu Rev Env Resour 2014;39:327-62.

570 [27] Yin F, Hou D, Liu W, Deng Y. Novel assessment and countermeasure for micro-annulus initiation of cement sheath during

571   injection/fracturing. Fuel 2019;252(15):157-63.

572 [28] McLaughlin MC, Borch T, Blotevogel J. Spills of hydraulic fracturing chemicals on agricultural topsoil: Biodegradation, sorption, and

573   co-contaminant interactions. Environ Sci Technol 2016;50:6071-78.

574 [29] Chen SS, Sun Y, Tsang DCW, Graham NJD, Ok YS, Feng Y, Li XD. Potential impact of flowback water from hydraulic fracturing on

575   agricultural soil quality: Metal/metalloid bioaccessibility, microtox bioassay, and enzyme activities. Sci Total Environ 2017;579:1419-

576   26.

577 [30] Faber AH, Annevelink MPJA, Schot PP, Baken KA, Schriks M, Emke E, de Voogt P, van Wezel AP. Chemical and bioassay assessment

578   of waters related to hydraulic fracturing at a tight gas production site. Sci Total Environ 2019;690:636-46.

579   [31] Andrews IJ. The Carboniferous Bowland Shale gas study: geology and resource estimation. British Geological Survey 2013.

580   [32] Waters CN, Browne MAE, Dean MT, Powell JH. Lithostratigraphical framework for Carboniferous successions of Great Britain
581   (Onshore). British Geological Survey, Keyworth, Nottingham, UK, 2007.

582   [33] Fraser AJ, Nash DF, Steele RP, Ebdon CC. A regional assessment of the intra-Carboniferous play of Northern England. Geol Soc London
583   Spec Publ 1995;50:417-40.

584   [34] Hough E, Vane CH, Smith NJP, Moss-Hayes VL. The bowland shale in the roosecote borehole of the lancaster fells sub-basin, craven
585   basin, UK: a potential UK shale gas play? SPE International, SPE167696, 2014.

586   [35] Hennissen JAI, Gent CMA. Total organic carbon in the bowland-hodder unit of the southern widmerpool gulf: a discussion. J Petrol Sci
587   Eng 2019;178:1194-202.

588   [36] Gu Y. Automated scanning electron microscope based mineral liberation analysis. J Miner Mater Char Eng 2003;2:33-41.

589   [37] Aminto A, Olson MS. Four-compartment partition model of hazardous components in hydraulic fracturing fluid additives. J Nat Gas Sci
590   Eng 2012;7:16-21.

591   [38] Lavergren U, Åström ME, Bergbäck B, Holmström H. Mobility of trace elements in black shale assessed by leaching tests and sequential
592   chemical extraction. Geochem-Explor Env A 2009;9:71-9.

593   [39] Li QY, Jew AD, Kohli A, Maher K, Jr GEB, Bargar JR. Thickness of chemically altered zones in shale matrices resulting from interactions
594   with hydraulic fracturing fluid. Energy Fuels 2019;33:6878-89.

595   [40] Chandra AP, Gerson AR. The mechanisms of pyrite oxidation and leaching: a fundamental perspective. Surf Sci Rep 2010;65(9):293-
596   315.

597   [41] Pilewski J, Sharma S, Agrawal V, Hakala JA, Stuckman MY. Effect of maturity and mineralogy on fluid-rock reactions in the marcellus
598   shale. Env. Sci.: Processes and Impacts 2019;21:845-55.

599   [42] Rimstidt JD, Vaughan DJ. Pyrite oxidation: a state-of-the-art assessment of the reaction mechanism. Geochim Cosmochim Ac
600   2003;67(5):873-80.

601   [43] Jew AD, Dustin MK, Harrison AL, Joe-Wong CM, Thomas DL, Maher K, Brown GE, Bargar JR. Impact of organics and carbonates on
602   the oxidation and precipitation of iron during hydraulic fracturing of shale. Energy Fuels 2017;31:3643-58.

603   [44] Simón M, Martín F, García I, Bouza P, Dorronsoro C, Aguilar J. Interaction of limestone grains and acidic solutions from the oxidation
604   of pyrite tailings. Environ Pollut 2005;135(1):65-72.

605   [45] Williamson MA, Rimstidt JD. The kinetics and electrochemical rate-determining step of aqueous pyrite oxidation. Geochim Cosmochim
606   Ac 1994;58(24):5443-54.

607   [46] Moses CO, Nordstrom DK, Herman JS, Mills AL. Aqueous pyrite oxidation by dissolved oxygen and by ferric iron. Geochim
608   Cosmochim Ac 1987;51(6):1561-71.

609   [47] Wei X, ViaderoJr RC, Buzby KM. Recovery of iron and aluminium from acid mine drainage by selective precipitation. Environ Eng Sci
610   2005;22(6):745-55.

611   [48] Dustin MK, Bargar JR, Jew AD, Harrison AL, Joe-Wong C, Thomas DL, Brown JrGE, Maher K. Shale kerogen: hydraulic fracturing
612   fluid interactions and contaminant release. Energy Fuels 2018;32:8966-77.

[49] Piszcz-Karaś K, Łuczak J, Hupka J. Release of selected chemical elements from shale drill cuttings to aqueous solutions of different pH. Appl Geochem 2016;72:136-45.

[50] Palandri JL, Kharaka YK. A compilation of rate parameters of water-mineral interaction kinetics for application to geochemical modelling. U. S. Geological Survey. Open File Report 2004.

[51] Wada N, Yamashita K, Umegaki T. Effects of divalent cations upon nucleation, growth and transformation of calcium carbonate polymorphs under conditions of double diffusion. J Cryst Growth 1995;148(3):297-304.

[52] Chou L, Garrels RM, Wollast R. Comparative study of the kinetics and mechanisms of dissolution of carbonate minerals. Chem Geol 1989;78:269-82.

[53] Lee G, Bigham JM, Faure G. Removal of trace metals by coprecipitation with Fe, Al, and Mn from natural waters contaminated with acid mine drainage in the Ducktown Mining District, Tennessee. Appl Geochem 2002;17(5):569-81.

[54] Shand P, Edmunds WM, Lawrence AR, Smedley PL, Burke S. The natural (baseline) quality of groundwater in England and Wales. British Geological Survey and Environment Agency 2007.

[55] Balintova M, Petrilakova A. Study of pH influence of selective precipitation of heavy metals from acid mine drainage. Chem Eng Trans 2011; 25:1-6.

[56] Titschack J, Goetz-Neunhoeffer F, Neubauer J. Magnesium quantification in calcites [(Ca,Mg)CO$_3$] by Rietveld-based XRD analysis: Revisiting a well-established method. Am Mineral 2011;96(7):1028-38.

[57] Lasaga AC. Chemical kinetics of water-rock interactions. J Geophys Res 1984;89:4009-25.

[58] Kirby CS, Dennis A, Kahler A. Aeration to degas CO_2, increase pH, and increase iron oxidation rates for efficient treatment of net alkaline mine drainage. Appl Geochem 2009;24(7):1175-84.

[59] Seo EY, Cheong YW, Yim GJ, Min KW, Geroni JN. Recovery of Fe, Al and Mn in acid coal mine drainage by sequential selective precipitation with control of pH. CATENA 2017;148(1):11-6.

[60] Pearce JK, Turner L, Pandey D. Experimental and predicted geochemical shale-water reactions: Roseneath and Murteree shales of the Cooper Basin. Int J Coal Geol 2018;187:30-44.

[61] Mucci A. Manganese uptake during calcite precipitation from seawater: Conditions leading to the formation of a pseudokutnahorite. Geochim Cosmochim Ac 1988;52(7):1859-68.

[62] Pingitore NE, Eastman MP, Sandidge M, Oden K, Freiha B. The coprecipitation of manganese(II) with calcite: an experimental study. Mar Chem 1988;25(2):107-20.

[63] Rose AW, Means B, Shah PJ. Methods for passive removal of manganese from acid mine drainage. In: Proceedings of the 24th WV surface mine drainage task force symposium, Morgantown, WV 2003.

[64] Patrick WHJr, Henderson RE. Reduction and reoxidation cycles of manganese and iron in flooded soil and in water solution. Soil Sci Soc Am J 1981;45:855-9.

[65] Evangelou VP, Zhang YL. A review: pyrite oxidation mechanisms and acid mine drainage prevention. Crit Rev Env Sci Tec 1995;25(2):141-99.

[66] Renock D, Landis JD, Sharma M. Reductive weathering of black shale and release of barium during hydraulic fracturing. Appl Geochem

647   2016;65:73-86.

648   [67] Carbonell AA, Pulido R, DeLaune RD, Patrick WHJr. Soluble barium in barite and phosphogypsum amended mississippi river alluvial

649   sediment. J Environ Qual 1999;28:316-21.

650   [68] Kolker A, Nordstrom DK. Occurrence and micro-distribution of arsenic in pyrite. USGS workshop on arsenic in the environment. Denver,

651   USA 2001.

652   [69] Blanchard M, Alfredsson M, Brodholt J, Wright K, Catlow RA. Arsenic incorporation in to FeS_2 pyrite and its influence on dissolution:

653   A DFT study. Geochim Cosmochim Ac 2007;71(3):624-30.

654   [70] Kreisserman Y, Emmanuel S. Release of particulate iron sulphide during shale-fluid interaction. Environ Sci Technol 2018;52:638-43.

655   [71] Tesoriero AJ, Pankow JF. Solid solution partitioning of Sr^{2+}, Ba^{2+}, and Cd^{2+} to calcite. Geochim Cosmochim Ac 1996;60(6):1053-63.

656   [72] Eloussaief M, Jarraya I, Benzina M. Adsorption of copper ions on two clays from Tunisia: pH and temperature effects. Appl Clay Sci

657   2009;46:409-13.

658   [73] Huang P, Fuerstenau DW. The effect of the adsorption of lead and cadmium ions on the interfacial behavior of quartz and talc. Colloid

659   Surface A 2001;177(2-3):147-56.

660   [74] He H, Guo J, Xie X, Peng J. Experimental study of the selective adsorption of heavy metals onto clay minerals. Chin J Geochem

661   2000;19(2):105-9.

662   [75] Li LY, Li RS. The role of clay minerals and the effect of H^+ ions on removal of heavy metal (Pb^{2+}) from contaminated soils. Can

663   Geotech J 2000;37(2):296-307.

664   [76] McBride RM. Environmental chemistry of soils. Oxford: Oxford University Press 1994.

665   [77] Atun G, Bascetin E. Adsorption of barium on kaolinite, illite and montmorillonite at various ionic strengths. Radiochimi Acta

666   2003;91:223-8.

667   [78] Hidaka H, Horie K, Gauthier-Lafaye F. Transport and selective uptake of radium into natural clay minerals. Earth Planet Sci Lett

668   2007;264(1-2):167-76.

669   [79] Dong D, Nelson YM, Lion LW, Shuler ML, Ghiorse WC. Adsorption of Pb and Cd onto metal oxides and organic material in natural

670   surface coatings as determined by selective extractions: new evidence for the importance of Mn and Fe oxides. Water Res

671   2000;34(2):427-36.

672   [80] Ghanbari E, Dehghanpour H. Impact of rock fabric on water imbibition and salt diffusion in gas shale. Int J Coal Geol 2015;138:55-67.

673   [81] Chen Q, Kang Y, You L, Yang P, Zhang X, Cheng Q. Change in composition and pore structure of Longmaxi black shale during oxidative

674   dissolution. Int J Coal Geol 2017;172:95-111.

675   [82] Dehghanpour H, Lan Q, Saeed Y, Fei H, Qi Z. Spontaneous imbibition of brine and oil in gas shale: effects of water adsorption and

676   resulting microfractures. Energy Fuels 2013;27:3039-49.

677   [83] Wang Y, Liu X, Liang L, Xiong J. Experimental study on the damage of organic-rich shale during water-shale interaction. J Nat Gas Sci

678   Eng 2020;74:103103.

679   [84] Chenevert ME. Shale alteration by water adsorption. J Pet Technol 1970;22:1141-8.

680   [85] Renard F, Bernard D, Desrues J, Ougier-Simonin A. 3D imaging of fracture propagation using synchrotron X-ray microtomography.

681   Earth Planet Sci Lett 2009;286:285-91.

682 [86] Yoshiya K, Nishizawa M, Sawaki Y, Ueno Y, Komiya T, Yamada K, Yoshida N, Hirata T, Wada H, Maruyama S. In situ iron isotope

683   analyses of pyrite and organic carbon isotope ratios in the Fortescue Group: Metabolic variations of a Late Archean ecosystem.

684   Precambrian Res 2012;212-213:169-93.

685 [87] World Health Organization, 2017. Guidelines for drinking-water quality: fourth edition incorporating the first addendum. World Health

686   Organization, Geneva.

687

List of Figures

Fig. 1. The Roosecote 1 Borehole. A: chrono- and lithostratigraphy alongside the downhole gamma response [31,34] with indication of sample depths; B: Carboniferous palaeogeography of the Pennine Basin with location of the Roosecote 1 Borehole; C: Idealized cross-section throught the Millstone Grit and Bowland Hodder Unit as a key for the schematic colouring of A (following Hennissen and Gent [35] modification of Andrews [31]). Csrt. = chronostratigraphy, Quat. = Quaternary.

Fig. 2. Powder X-Ray Diffractograms: I=illite; Q=quartz; C=calcite; P=pyrite.

Fig. 3. MLA image of shale samples before reaction: (a) MLA measurement of RC618; (b) MLA measurement of RC673.

Fig. 4. pH before and after (100 h) water/rock interaction (RC618).

Fig. 5. pH before and after (100 h) water/rock interaction (RC673).

Fig. 6. Elemental composition of the fluids in the experiments with RC618 at different test conditions after 100 hours reaction time.

Fig. 7. Elemental composition of the fluids in the experiments with RC673 at different test conditions after 100 hours reaction time.

Fig. 8. Mg mobilisation under different experimental scenarios after 100 hours reaction time: (a) Mg vs. Al concentration in RC618; (b) Mg vs. Ca concentration in RC673.

Fig. 9. Elemental mobilisation for RC618 and RC673 (0.1 mol/L HCl) at temperatures of 25-70 °C: (a) Fe mobilisation through reaction time; (b) Al mobilisation through reaction time; (c) Ca mobilisation through reaction time.

Fig. 10. Trace element mobilisation under different acid concentrations at temperatures of 60 °C with a constant rock/fluid ratio of 2 g: 200 mL: (a) elemental mobilisation in experiments with RC618; (b) elemental mobilisation in experiments with RC673.

Fig. 11. As and Sr mobilisation under different experimental scenarios after 100 hours reaction time: (a) As vs. Fe concentration in RC618; (b) Sr vs. Ca concentration.

Fig. 12. Trace element mobilisation under different temperatures at acid concentration of 0.1 mol/L HCl with a constant rock/fluid ratio of 2 g: 200 mL: (a) elemental mobilisation in experiments with RC618; (b) elemental mobilisation in experiments with RC673.

Fig. 13. Trace element mobilisation at different rock/fluid ratios, temperature of 60 °C and acid concentration of 0.1 mol/L HCl: (a) elemental mobilisation in experiments with RC618; (b) elemental mobilisation in experiments with RC673.

Fig. 14. MLA image of shale samples after reaction: (a) MLA measurement of RC618; (b) MLA measurement of RC673.

Fig. 15. SEM images of the different minerals morphology before and after reaction (100 h) with acidic fluid: (a-d) SEM images of RC618; (e-h) SEM images of RC673.

Fig. 16. 3D colour surface profiles of different minerals after acidic treatment in shale RC618 and RC673.

List of Tables

715

716 **Table 1** Summary of experiments (elemental analysis).

717 **Table 2** Summary of experiments (MLA and SEM analyses).

718 **Table 3** MLA data of shale RC618 and RC673 before reaction.

719 **Table 4** MLA data of shale RC618 and RC673 after reaction.